This article has been accepted for publication in IEEE Transactions on Power Systems. This is the author's version which has not been fully edited and content may change prior to final publication. Citation information: DOI 10.1109/TPWRS.2023.3330604

Impact of Backlash Nonlinearity on the Dynamics of Type-3 Turbine-based Windfarms

Abdul Saleem Mir, Abhinav Kumar Singh, Bikash C. Pal and Nilanjan Senroy

***Abstract*— This paper considers detailed modeling of gear backlash in the drivetrains of a type-3 turbine-based windfarm in an interconnected power system. The detailed model has been used to: (*a*) thoroughly investigate the impact of backlash on the dynamic performance and response of the windfarm; (*b*) identify the nature of various modes and the change of the modal properties with changes in system parameters and operating conditions through eigenvalue analysis; and (*c*) study the effect of traditional lead-lag and linear quadratic stabilizers on oscillation suppression, particularly blade vibrations. Novel indices and realistic wind speed profile simulated using Van'der Hoven spectrum have been used to study the impact of backlash and variation in its width on the dynamic performance of the wind farm. Also, inadequacies in existing models of type-3 turbines have been identified in terms of control design.**

***Index Terms*— windfarm, wind turbine generator (WTG), doubly-fed-induction-generator (DFIG), modal analysis, nonlinear modeling, structure, backlash, vibrations.**

NOMENCLATURE

i, k	General subscript for the i^{th} or the k^{th} unit resp.
ω_s, ω_{B}	Synchronous speed, base elec. speed (rad./s) resp.
ω_r, ω_t	DFIG rotor and turbine speeds in (rad./s) resp.
E'_q, E'_d	Equivalent source voltages along q and d axis resp.
I_{qs}, I_{ds}	Quadrature/direct axis stator currents in *p.u.* resp.
V_{qr}, V_{dr}	Quadrature/direct axis rotor voltages in *p.u.* resp.
I_{qr}, I_{dr}	Quadrature/direct axis rotor currents in *p.u.* resp.
V_{qs}, V_{ds}	Quadrature/direct axis stator voltages in *p.u.* resp.
V_{qg}, V_{dg}	Quadrature/direct axis GSC voltages in *p.u.* resp.
I_{qg}, I_{dg}	Quadrature/direct axis GSC currents in *p.u.* resp.
R_s, R_r	DFIG stator and rotor resistances resp.
V_{DC}, C	DFIG DC link voltage and capacitance resp.
H_t, H_g	Turbine and DFIG inertia constants respectively.
c_{sh}, k_{sh}	Shaft damping and stiffness coefficients.
θ_{tw}	Shaft twist angle between DFIG and turbine shafts
n_s	Number of synchronous machine in the test system
n_w	Number of wind turbine units in the windfarm.
P_e^*, P_e	DFIG reference and actual electrical power outputs
Q_S^*, Q_S	DFIG stator ref. and actual reactive power outputs
$\mathrm{Q}_{\mathrm{GSC}}$	Grid side converter reactive power output
$\mathrm{Q}^*_{\mathrm{GSC}}$	Grid side converter reference reactive power
θ_{pl}	DFIG phase locked loop angle.
x_{pl1}	PLL state 1, x_{pl2} PLL state 2
x_{P}, $x_{\mathrm{I}_{qr}}$	RSC active power control loop states
x_{Q}, $x_{\mathrm{I}_{dr}}$	RSC reactive power control loop states
$x_{\mathrm{V}_{\mathrm{DC}}}$	GSC DC link voltage control loop state
$x_{\mathrm{Q}_{\mathrm{GSC}}}$	GSC reactive power control loop state
V_{pcw}	Windfarm interconnection point voltage magnitude
γ_{pcw}	Windfarm interconnection point voltage phase
Z_{w}	DFIG unit impedance
ϱ	Backlash/dead-zone width
$\boldsymbol{\xi}$	Wind turbine structural state vector
f_b	Net tangential force on the blade
f_t	Net force on the tower due to wind
$f_{Ti}(l,t)$	Net tangential force on structural element
β, τ_{B}	Pitch angle and corresponding loop time constant
k_{wr}	Pitch angle control loop gain
v_w	Wind speed (ms^{-1})
V_t	Terminal voltage (*p.u.*)
$\dot{\omega}_{ti}$	Turbine acceleration ($rad./s^2$)
g	Acceleration due to gravity
X_C	GSC transformer reactance in *p.u.*
I_{w}	Injected current from a DFIG-WTG unit
R_a	Synchronous machine stator resistance in *p.u.*
x''_d	Synchronous machine subtransient reactance in *p.u*
δ	Synchronous machine rotor angle (radians)
ω	Synchronous machine speed (rad./s)

I. INTRODUCTION

POWER from renewable sources of energy, like wind, account for one-third of the total power generation capacity of the world as of 2019 and it is anticipated to increase significantly in the next decade [1]-[2]. Type-3 wind turbine generators (WTGs) are being increasingly used to harness energy from wind. The increased share of power from type-3 WTGs has led to new types of grid stability challenges and bulk penetration tends to amplify their impact [3]-[7]. These problems arise due to the asynchronous and low-inertia nature, and largely different dynamic behavior of doubly-fed-induction-machines deployed with type-3 WTGs compared to that of synchronous machines [5].

Power oscillation related events leading to eventual tripping of wind turbine units have been reported in the power system literature [5], [8]. The accuracy of dynamic studies pertaining to these oscillations in modern power systems relies heavily on the underlying model fidelity /adequacy of the components. In this context, type-3 WTG modeling has garnered considerable attention of the power

This work was partially supported by EPSRC UK under Grant EP/T021713/1, FIG-IITR (EED/FIG/100967) and SERB-SRG under Grant SRG/2023/000405.

Abdul Saleem Mir is with the Department of Electrical Engineering, Indian Institute of Technology Roorkee, Roorkee 247667, India (e-mail: saleemmir@ee.iitr.ac.in).

Abhinav Kumar Singh is with the School of Electronics and Computer Science, University of Southampton, SO17 1BJ Southampton, U.K. (e-mail: a.k.singh@soton.ac.uk).

Bikash C. Pal is with the Department of Electrical and Electronic Engineering, Imperial College London, SW7 2BX London, U.K. (e-mail: b.pal@imperial.ac.uk).

Nilanjan Senroy is with the Department of Electrical Engineering, Indian Institute of Technology Delhi, Delhi 110016, India (e-mail: nsenroy@ee.iitd.ac.in).

Authorized licensed use limited to: UNIVERSITY OF SOUTHAMPTON. Downloaded on February 13,2024 at 09:11:53 UTC from IEEE Xplore. Restrictions apply.
© 2023 IEEE. Personal use is permitted, but republication/redistribution requires IEEE permission. See https://www.ieee.org/publications/rights/index.html for more information.

This article has been accepted for publication in IEEE Transactions on Power Systems. This is the author's version which has not been fully edited and content may change prior to final publication. Citation information: DOI 10.1109/TPWRS.2023.3330604

system researchers [4]-[10]. The dynamic simulations of type-3 WTGs based windfarm with horizontal-axis-wind-turbine (HAWT) arrangement has been extensively investigated. Specifically, decoupled active and reactive power control [11], simplistic modeling based integration studies [12], investigation/evaluation of the standard vector control schemes for WTG operation in autonomous mode [13], control of HAWT with multi-mass modeling paradigms [14], decoupled flux-magnitude-angle-control [15], deloading based primary frequency control [16] and analysis for dynamic studies with reduced order model [17] have been explored.

In the literature pertaining to Type-3 WTGs, researchers assume either detailed electrical and simplistic mechanical dynamics [7]-[15], or simplistic electrical and detailed mechanical dynamics [18]-[20]. Simulation based approach using tools like Turbulence-Simulator (TurbSim), NREL-FAST and Matlab/Simulink has been used to study wind turbine dynamic behavior [18]. Likewise, the evolution and control of structural dynamics using FAST based structural and aerodynamical subsystems has been reported in [21]. For inertial support [22] and fast frequency response [23], electromechanical models of the WTGs have been used. Similarly, blade bending dynamics has also been considered in [24]. However, the WTG models used in the existing literature do not consider structural dynamics and gear backlash nonlinearity, which may significantly affect the inertial/fast-frequency response. This is because, the wind turbine acceleration upon the inception of a network disturbance or change in the input wind speed induces/amplifies vibrations in the turbine structure, that is, in tower and blades. The modeling paradigm of [6] for examination of structural interactions in wind turbines overlooks the impact of system nonlinearities due to backlash and stochasticity of the input wind speed and has used an open loop grid connected system for the study. Likewise, pitch angle control and structural dynamics have not been considered in [25]-[26]. Moreover, the backlash model used in [26] introduces more intermediate variables. Additionally, majority of existing studies consider simplified aggregate windfarm models and conclusions drawn may not be accurate or reliable [27]-[28]. The impact of the phase locked loops on the low frequency oscillations has been explored in [29]. Similarly, the impact of various PLL parameters on the transient stability of DFIG based WTGs using approximate models has been studied in [30], [31]. The transient response of DFIG based wind turbines in the rotor speed timescale has been analyzed in [32]. Similarly, damping [33] and inertia emulation [34] controllers have been proposed for DFIGs while representing its dynamics by electromechanical models with standard converter control architectures. The majority of these studies do not consider system nonlinearities such as backlash and ignore the structural dynamics completely.

To address the above issues, the dynamic performance of a windfarm with type-3 doubly fed induction generator (DFIG) based WTGs considering detailed modeling of gear-backlash nonlinearities, structural dynamics and stochastic wind speed has been investigated in this paper. The primary contributions of this paper are as follows:

1. Considering a unified electrical, mechanical, and structural model with backlash nonlinearity for type-3 WTG based windfarm in an interconnected power system. Unlike models of type-3 wind turbine generators in the literature, this is most detailed and complete model of a Type-3 WTG based windfarm.
2. An analytical expression has been obtained for the turbine force due to turbine acceleration. This expression is not available anywhere in the literature. Additionally, we have proposed two indices to quantitatively gauge the impact of backlash on the overall dynamics of Type-3 WTGs in power systems.
3. Conducting detailed stability analysis in a multimachine environment to understand the modal nature/interactions of the windfarm considering backlash nonlinearity, and impact of change in system parameters and grid conditions, for designing appropriate control schemes.
4. Studying the impact of gear backlash on the dynamic performance of type-3 WTGs in a power system. The findings suggest that the blade vibrations get amplified with gear backlash whereas the effect on other mechanical and electromechanical oscillations is also significant. Potential impacts of these amplifications include increased blade stress and possible structural failures.
5. Finding the effects of traditional damping controllers [9], [15] on oscillation suppression, particularly blade vibrations, and identifying the modeling inadequacies in traditional control design.
6. Studying the impact of backlash nonlinearity on the system frequency at the point of interconnection. The inadequacy of the aggregate model [35]-[36] in comparison to the detailed model introduced has also been shown.

The eigenvalue findings are supported by time domain simulations and Fourier analysis of the corresponding time-response. Realistic wind speed profiles based on Van'der Hoven spectrum [37] have been used to perform various tests.

The rest of the paper is structured as follows. The modeling of power system components has been briefly discussed in Section II. Wind turbine structural dynamics and wind speed model has been discussed in Section III. The physics behind dynamical interaction and backlash nonlinearity is presented in Section IV. The case study, which includes linear analysis and time-domain simulations, has been presented in Section V. Section VI respectively present the impact of auxiliary damping controls in light of backlash. Section VII concisely discusses the impact of backlash on frequency stability, while Section VIII discusses the findings of this paper. The conclusions and the future scope have been presented in Section IX.

II. WINDFARM MODELING

Instead of representing the entire windfarm as a simplified aggregated model, which is a gross approximation, the windfarm consists of n_w number of DFIG based wind turbine units (for the case study in Section V, $n_w = 50$). The most commonly used configuration for large utility-scale windfarms is shown in Fig. 1. The windfarm (rated 250MW) consists of five strings with ten

Authorized licensed use limited to: UNIVERSITY OF SOUTHAMPTON. Downloaded on February 13,2024 at 09:11:53 UTC from IEEE Xplore. Restrictions apply.
© 2023 IEEE. Personal use is permitted, but republication/redistribution requires IEEE permission. See https://www.ieee.org/publications/rights/index.html for more information.

This article has been accepted for publication in IEEE Transactions on Power Systems. This is the author's version which has not been fully edited and content may change prior to final publication. Citation information: DOI 10.1109/TPWRS.2023.3330604

WTGs units in each string. The power from various strings is collected at the medium voltage bus bar. In this configuration the voltage level is further stepped up to high-voltage by a medium voltage to high voltage (MV/HV) transformer for its coupling to the transmission grid. An individual WTG unit with rated power of 5MW comprises of a DFIG, a drive train and a tower structure with blades. The dynamics of an i^{th} WTG unit of the windfarm (Fig. 2) is given by a system of differential-algebraic-equations given in Appendix-A (A1)-(A12).

Converter Control, PLL dynamics, dq-frame alignment [42]

The grid-side converter and the machine side converter of the DFIG use a cascaded control paradigm [7], [41]-[42]. Phase locked loop (PLL) for synchronization of a DFIG unit with the grid is represented by following set of equations (1)-(3). The PLL angle θ_{pli} is used for dq-frame alignment [42].

$$\dot{x}_{pli2} = k_{pli2}x_{pli2} \quad (1)$$

$$\dot{\theta}_{pli} = k_{pli3}x_{pli1} + x_{pli2} \quad (2)$$

$$\dot{x}_{pli1} = k_{pli1}\left[Im\left((V_{qsi} + jV_{dsi})e^{-j\theta_{pli}}\right) - x_{pli1}\right] \quad (3)$$

Grid Integration and Network representation [40], [43]

The transmission network is represented by node algebraic equations [43]. The transmission lines and transformers are represented by equivalent π-models. The node equations of the network and loads are represented by (4).

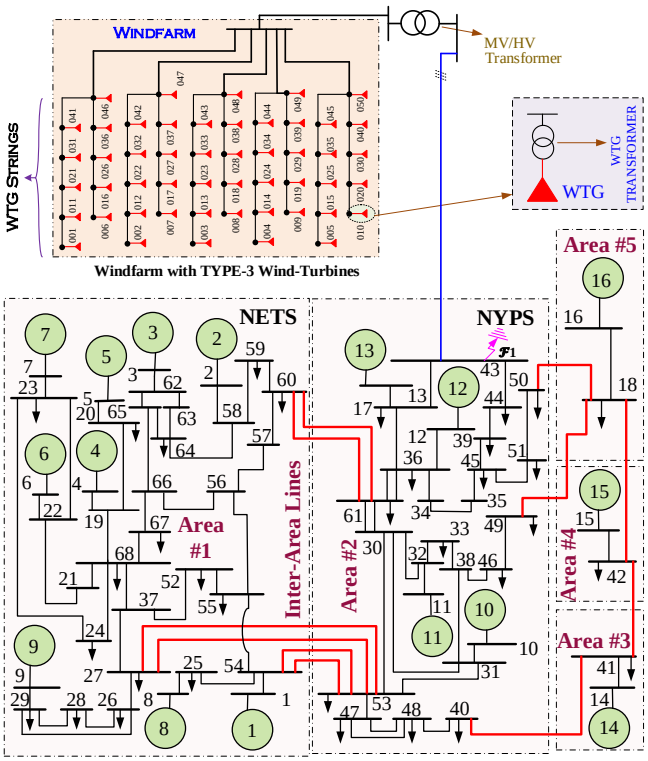

Fig. 1: Test system [38] with Type-3 WTG based windfarm interconnection

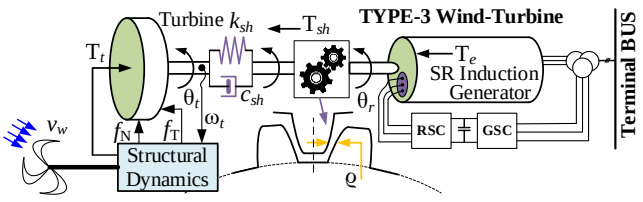

Fig. 2: Type-3 wind turbine generator

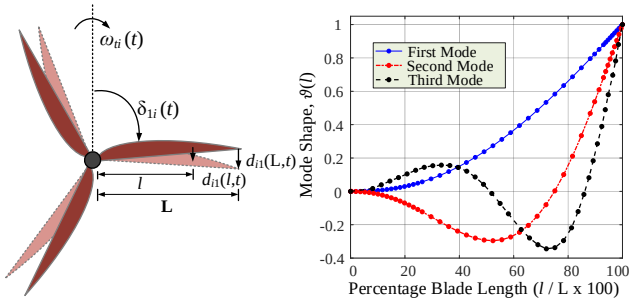

Fig. 3: (*a*) Edgewise vibration of blades (*b*) Mode shapes

$$\mathbf{V} = \mathbf{Z_{AUG}}\mathbf{I}\ ,\ \mathbf{Z_{AUG}} = \mathbf{Y_{AUG}^{-1}} \quad (4)$$

where, $\mathbf{Y_{AUG}} = \mathbf{Y_G} + \mathbf{Y_N} + \mathbf{Y_L}$, $\mathbf{Y_G} = diag(\mathrm{Y_{G1}}, \mathrm{Y_{G2}}, \dots, \mathrm{Y_{GN}})$, $\mathrm{Y_{G}}_j = (R_{ai} + jx''_{di})^{-1}$ when i^{th} synchronous generator is connected to j^{th} network node, otherwise $\mathrm{Y_{G}}_j = 0$. If a single WTG unit is connected to the j^{th} network node then $\mathrm{Y_{G}}_j = 1/\mathrm{Z_{W}}_i$ and if n_x WTG units are connected to j^{th} network node then $\mathrm{Y_{G}}_j = \sum_{i=1}^{n_w}(1./\mathrm{Z_{W}}_i)$. $\mathbf{Y_N}$ is the network shunt admittance and $\mathbf{Y_L}$ is load admittance matrix.

For a type-3 WTG, the current injected to the network is the sum of the GSC ac-current and stator current (5). The PLL angle θ_{pli} is used for reference frame realignment of DFIG voltages/currents [43]. The corresponding equation of the DFIG stator voltage of an i^{th} WTG is given by (6).

$$I_{wi} = I_{qsi} + jI_{dsi} + I_{qgi} + jI_{dgi} \quad (5)$$

$$\mathrm{V}_{qsi} + j\mathrm{V}_{dsi} = \mathrm{V}_{pcw}\angle\gamma_{pcw} + jI_{wi}\mathrm{Z}_{wi} \quad (6)$$

Pitch Angle Control [41]

When the wind speed exceeds the WTG rating, the mechanical torque developed is limited by blade pitching mechanism as follows:

$$\beta_i^* = k_{wri}(\omega_{ri}^* - \omega_{ri}) \quad (7)$$

$$\tau_{Bi}\dot{\beta}_i = \beta_i^* - \beta_i \quad (8)$$

Drive Train Model of the Turbine-DFIG [7], [41]

The basic power balance equations of the drive train in per unit for i^{th} turbine of the wind-farm are written as shown in Appendix-A (A8)-(A10).

Backlash Models [44]-[45]

Two types of mathematical models can be used to represent the gear backlash nonlinearity in the drive-train architecture of the type-3 WTGs, which have been described below.

Dead-Zone Model

The backlash may be modelled as a dead-zone for simulation/analysis. The shaft torque T_{shi} in equation (A11) is modified as (9) to include the gear backlash as dead-zone with width equal to $2\varrho_i$.

$$T_{shi} = \begin{cases} k_{shi}(\theta_{twi} - \varrho_i) + c_{shi}\dot{\theta}_{twi} & m_{si} > \varrho_i \\ 0 & |m_{si}| \le \varrho_i \\ k_{shi}(\theta_{twi} + \varrho_i) + c_{shi}\dot{\theta}_{twi} & m_{si} < -\varrho_i \end{cases} \quad (9)$$

where, $m_{si} = \theta_{twi} + c_{shi}k_{shi}^{-1}\dot{\theta}_{twi}$.

Exact Model

Alternatively, the backlash may be described by the relation between twist angle θ_{tw}, turbine and generator speeds (ω_t *and* ω_r, respectively) and their angular positions (θ_t and θ_r, respectively, in Fig. 2). The shaft torque T_{shi} in equation (A11) is modified as (10) to incorporate the exact model of the backlash nonlinearity.

Authorized licensed use limited to: UNIVERSITY OF SOUTHAMPTON. Downloaded on February 13,2024 at 09:11:53 UTC from IEEE Xplore. Restrictions apply.
© 2023 IEEE. Personal use is permitted, but republication/redistribution requires IEEE permission. See https://www.ieee.org/publications/rights/index.html for more information.

This article has been accepted for publication in IEEE Transactions on Power Systems. This is the author's version which has not been fully edited and content may change prior to final publication. Citation information: DOI 10.1109/TPWRS.2023.3330604

$$T_{shi} = k_{shi}(\theta_{twi} - \theta_{bi}) + c_{shi}\left(\dot{\theta}_{twi} - \dot{\theta}_{bi}\right) \quad (10)$$

with,

$$\dot{\theta}_{bi} = \begin{cases} \max(0, \dot{\theta}_{twi} + c_{shi}k_{shi}^{-1}(\theta_{twi} - \theta_{bi})) & if\ \theta_{bi} = -\varrho_i \\ \dot{\theta}_{twi} + c_{shi}k_{shi}^{-1}(\theta_{twi} - \theta_{bi}) & if\ |\theta_{bi}| < \varrho_i \\ \min(0, \dot{\theta}_{twi} + c_{shi}k_{shi}^{-1}(\theta_{twi} - \theta_{bi})) & if\ \theta_{bi} = \varrho_i \end{cases} \quad (11)$$

where, θ_{bi} is the dead-band angle. The exact model of the (11) has been used in this paper as it is physically more accurate and uses minimal assumptions in its derivation [44]-[46].

IV. Structural Dynamics and Wind Speed Model

Modeling of the Wind Turbine Structure

The schematic of the rotor of the i^{th} horizontal-axis-wind-turbine of the windfarm for the modeling of the edgewise blade vibrations is shown in Fig. 3 (a).

The speed of the turbine is $\omega_{ti}(rad/s)$ whereas the angle of the k^{th} blade, $\delta_{ki}\ (rad)$ with respect to the vertical axis is given by (12).

$$\delta_{ki}(t) = \omega_{ti}t + (k-1)2\pi/3\ ,\ k = 1,2,3 \quad (12)$$

The vibrations of the wind turbine structure are simulated by considering the rotor blades and the tower structure as flexible rotating and fixed beams, respectively, with edgewise vibration mode shapes $\vartheta(l)$ (Fig. 3 (b)). In this paper, a single vibration mode (first-mode of Fig. 3 (b)) has been considered as it adequately and appropriately represents the blade vibrations of significant concern [46]. The displacement of the three blades from the hub at a fractional distance l/L is $d_{ik}(l,t)\ , k = 1,2,3$, whereas the displacement of the tower-top is $d_{i4}(t)$. The edgewise blade vibration is described by a generic variable $\xi_{ik}(t), k = 1,2,3$, whereas the tower-top vibration is represented by $\xi_{i4}(t)$. At blade tips, the mode shape $\vartheta(l) = 1$, therefore, the generalized variable $\xi_{ik}(t), k = 1,2,3$, represents the tip edgewise vibration of the k^{th} blade. The total edgewise/lateral displacement along the blade is written as follows [19]-[20].

$$d_{ik}(l,t) = \vartheta(l)\xi_{ik}(t) \quad (13)$$

where, $\vartheta(l) = -0.69(l/L)^6 + 2.38(l/L)^5 - 3.58(l/L)^4 + 2.53(l/L)^3 + 0.36(l/L)^2$, $k = 1,2,3,4$ and $i = 1,\ldots,n_w$.

Using the Euler-Langrangian approach, the dynamical equations for the HAWT structure are modelled as [19]-[20].

$$\mathcal{M}_i(t)\ddot{\boldsymbol{\xi}}_i(t) + \mathcal{D}_i(t)\dot{\boldsymbol{\xi}}_i(t) + \mathcal{K}_i(t)\boldsymbol{\xi}_i(t) = \mathcal{F}_i(t) \quad (14)$$

$$\mathcal{F}_i(t) = \mathcal{F}_{\mathrm{W}i}(t) + \mathcal{F}_{\mathrm{G}i}(t) + \mathcal{F}_{\omega_{ti}}(t) \quad (15)$$

where, $\boldsymbol{\xi}_i = \left[\xi_{i1}\ \xi_{i2}\ \xi_{i3}\ \xi_{i4}\ \dot{\xi}_{i1}\ \dot{\xi}_{i2}\ \dot{\xi}_{i3}\ \dot{\xi}_{i4}\right]^{\mathrm{T}}$, $\mathcal{M}_i(t)$, $\mathcal{D}_i(t)$ and $\mathcal{K}_i(t)$ are time varying mass, damping and stiffness matrices of the wind turbine structure, respectively. $\mathcal{F}_{\mathrm{G}i}(t)$, $\mathcal{F}_{\mathrm{W}i}(t)$ and $\mathcal{F}_{\omega_{ti}}(t)$ are the tangential forces on the blades due to gravity, wind loading and the turbine acceleration, respectively.

$$\mathcal{F}_{\mathrm{W}i}(t) = [f_{bi}\ f_{bi}\ f_{bi}\ f_{ti}]^T \quad (16)$$

where,

$$f_{bi} = \int_0^L f_{Ti}(l,t)\vartheta(l)dl \quad (17)$$

$$f_{ti} = \sum_{k=1}^{3}\left(\int_0^L f_{Ti}(l,t)\cos\left(\delta_{ki}(t)\right)dl\right) \quad (18)$$

$$f_{Ti}(l,t) = \rho v_{rw}^2(l,t)\gamma(l)(\mathrm{K}_L\sin(\varphi) - \mathrm{K}_D\cos(\varphi))/2 \quad (19)$$

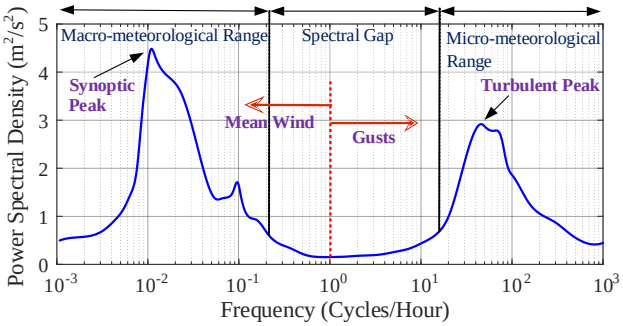

Fig. 4: Van'der-Hoven spectrum of the wind

where,

$$v_{rw}^2(l,t) \approx \left(v_w(1-i_{ai})\right)^2 + (\omega_{ti}l(1+i_{ti})^2) \quad (20)$$

$$\varphi(l,t) = atan\{v_w(1-i_{ai})/(\omega_{ti}l(1+i_{ti})\} \quad (21)$$

where, $f_{Ti}(l,t)$, f_{bi} and f_{ti} are, respectively, the net tangential force on each blade, the force per-unit-length on a blade element, and the net force on the tower-top due to the wind. ρ, $\gamma(l)$, $\mathrm{K}_L/\mathrm{K}_D$, i_{ai} and i_{ti} are, respectively, the air density, chord length of the blade at length l from the hub, lift/drag coefficients of the blade, axial and tangential induction factors. v_w is the instantaneous wind speed.

$$\mathcal{F}_{\mathrm{G}i}(t) = [f_{\mathrm{G}i1}\ f_{\mathrm{G}i2}\ f_{\mathrm{G}i3}\ f_{\mathrm{G}it}]^T \quad (22)$$

$$f_{Gik} = \mathrm{g}\int_0^L \sigma_m(l)\vartheta(l)\cos\left(\delta_{ki}(t)\right)dl\ ;\ k = 1,2,3 \quad (23)$$

where, $\sigma_m(l)$ is the linear mass density (specific mass) of the blade and $f_{\mathrm{G}it} = 0$.

$$\mathcal{F}_{\omega_{ti}}(t) = -\dot{\omega}_{ti}[\bar{\sigma}_m\ \bar{\sigma}_m\ \bar{\sigma}_m\ 0]^T \quad (24)$$

where, $\bar{\sigma}_m = \int_0^L \sigma_m(l)\vartheta(l)dl$.

Dynamic Wind Speed Model

The wind speed $v_w(t)$ when modelled using the Van'der-Hoven spectrum [37] (Fig. 4) properly captures its variability.

$$v_w(t) = \sum_{b=0}^{n} a_b\, cos(\omega_{sb}t + \phi_{sb}) + \sigma_v^2\omega_{gs}(t) \quad (25)$$

where

$$a_b = \pi^{-1}\left(2\left[S_v(\omega_{sb}) + S_v\left(\omega_{s(b+1)}\right)\right].\left[\omega_{s(b+1)} - \omega_{sb}\right]\right)^{1/2} \quad (26)$$

where, $b = 1{:}\ n+1$; n is the sample number. $S_v(\omega_{sb})$ is the spectral density (m^2/s^2) at an angular frequency ω_{si}, and $\phi_{sb} \in [\pi, -\pi]$ is the corresponding phase angle. $\omega_{gs}(t)$ is the coloured noise and σ_v^2 is the variance corresponding to average wind speed.

V. Backlash Nonlinearity and WTG Dynamics

The impact of gear backlash on windfarm dynamics can be understood via physics informed models used in this paper. The physics of backlash induced interactions is discussed below:

From (24) we have,

$$\mathcal{F}_{\omega_{ti}}(t) = -\dot{\omega}_{ti}\bar{\sigma}_M^{\mathrm{T}} \quad (27)$$

where, $\bar{\sigma}_M = [\bar{\sigma}_m\ \bar{\sigma}_m\ \bar{\sigma}_m\ 0]$. Using equations (A8), (9)-(11) the dependence of $\mathcal{F}_{\omega_{ti}}(t)$ on backlash width ϱ_i can be derived. Therefore,

$$\mathcal{F}_{\omega_{ti}}(t) = -(2H_{ti})^{-1}(T_{ti} - T_{shi})\bar{\sigma}_M^{\mathrm{T}} \quad (28)$$

The piecewise continuous function of the shaft torque T_{shi} given by (9) or (10) can be approximated by an equivalent differentiable backlash model [47] (29).

Authorized licensed use limited to: UNIVERSITY OF SOUTHAMPTON. Downloaded on February 13,2024 at 09:11:53 UTC from IEEE Xplore. Restrictions apply.
© 2023 IEEE. Personal use is permitted, but republication/redistribution requires IEEE permission. See https://www.ieee.org/publications/rights/index.html for more information.

This article has been accepted for publication in IEEE Transactions on Power Systems. This is the author's version which has not been fully edited and content may change prior to final publication. Citation information: DOI 10.1109/TPWRS.2023.3330604

$$T_{shi} = \frac{1}{\bar{\rho}} ln\left(\frac{1 + e^{\bar{\rho}k_{shi}(\theta_{twi} - \varrho_i)}}{1 + e^{-\bar{\rho}k_{shi}(\theta_{twi} + \varrho_i)}}\right) \quad (29)$$

where, $\bar{\rho}$ is a sufficiently large positive constant. Substituting the values of T_{shi} (29) and T_{ti} (A12) in (28), the dependence of vibration dynamics on wind speed variations and backlash width can be determined. Therefore,

$$\mathcal{F}_{\omega_{ti}} = -\left(k_i v_w^3 - S(\varrho_i)\right)\bar{\sigma}_{\mathrm{M}}^{\mathrm{T}}/2H_{ti} \quad (30)$$

where, $S(\varrho_i) = \frac{1}{\bar{\rho}} ln\left(\frac{1+e^{\bar{\rho}k_{shi}(\theta_{twi} - \varrho_i)}}{1+e^{-\bar{\rho}k_{shi}(\theta_{twi} + \varrho_i)}}\right)$, $k_i = k_{opt_i}$ when $\mathrm{C}_{p\ (p.u.)} = 1$ and $k_i = (\rho A \mathrm{C}_{pMAX} \mathrm{C}_{p\ (p.u.)} v_{w,Base}^3)/(2S_{\mathrm{WTG}})$ [41]. The terms S_{WTG}, C_{pMAX} and $v_{w,Base}$ represent the base value of WTG power, maximum value of power coefficient (C_p) and base wind speed respectively. Substituting (30) in (14)-(15), we get

$$\mathcal{M}_i(t)\ddot{\boldsymbol{\xi}}_i(t) + \mathcal{D}_i(t)\dot{\boldsymbol{\xi}}_i(t) + \mathcal{K}_i(t)\boldsymbol{\xi}_i(t) = \mathcal{F}_{\mathrm{W}i}(t) + \mathcal{F}_{Gi}(t) - \left(k_i v_w^3 - S(\varrho_i)\right)\bar{\sigma}_{\mathrm{M}}^{\mathrm{T}}/2H_{ti} \quad (31)$$

Deriving an exact (or even approximate) closed form expression for the impact of backlash on turbine vibrations and power output is mathematically infeasible without ignoring and incorrectly representing part of the nonlinear dynamics of wind turbines. However, a functional form can be obtained as in equations (27)-(31), which shows that the impact is ubiquitous irrespective of the parameters or the operating condition of the turbines, that is, the impact of backlash can be mild or severe depending on the operating condition, WTG parameters and the backlash bandwidth, but the impact will always be there. The severity of the impact can be quantified using the indices subsequently proposed in Section V.C.

Impact of Backlash on the Time Evolution of Structural Vibrations: The physical laws governing the structural dynamics of WTGs (14)-(15) illustrate that the time evolution of the vibration states of the WTG is a function of the net force $\mathcal{F}_i(t)$ on the WTG structure (14)-(15). This net force $\mathcal{F}_i(t)$ includes a component $\mathcal{F}_{\omega_{ti}}(t)$ which represents the tangential force on the turbine blades, induced due to acceleration of the turbine rotor. This force component (24), (27) is a function of two variables: 1) mass density vector "$\bar{\sigma}_M$" of the blade structure, and 2) turbine acceleration "$\dot{\omega}_{ti}$". The mass density is fixed for a given WTG structure. Therefore, the impact of this force component is primarily a function of turbine acceleration. The backlash reveals its impact in the shaft torque (10), (29) whenever the rotor speed changes or swings following an instantaneous mismatch between mechanical and electrical torques in the event of an input or network disturbance. As a result, the transmitting torque T_{shi} (10) becomes zero for a brief duration. During this duration, the teeth of the drive train gears are out-of-contact and the generator rotor oscillates as per the electromechanical dynamics of the WTG. Backlash causes accentuation of the turbine rotor acceleration $\dot{\omega}_{ti}$, therefore, it has an amplifying impact on $\mathcal{F}_{\omega_{ti}}(t)$ (30). Thus, the backlash induced oscillations in turbine speed translate into accentuated force on the turbine blades. As a result, it causes amplification of blade vibrations.

Backlash Width and Electromechanical Dynamics: Backlash in the drive train reveals itself whenever the adjacent teeth of the driving and the driven gears lose contact with each other. As a result, the transmitting torque T_{shi} (10) becomes zero whenever the gears are out-of-contact, and the generator rotor oscillates as per the electromechanical dynamics of the WTG (A8)-(A10). The backlash in WTGs is a mechanical phenomenon. It therefore has a direct influence on the time evolution of electromechanical states (θ_{twi}, ω_{ti}, ω_{ri}). As a result, it can cause the stimulation/excitation of the low frequency modes upon the inception of a disturbance. Moreover, the backlash also introduces lag in the time evolution of the electromechanical states due to uneven torque transmission and play between the driving and the driven gears (10) upon the inception of any disturbance. These inherent impacts of backlash are analytically investigated using a case study in the next section.

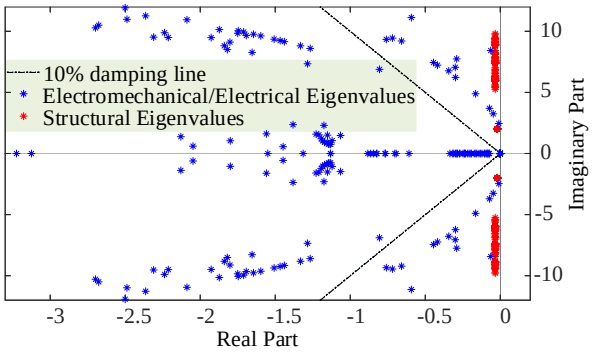

Fig. 5: Eigen-value plot of the test system with a windfarm.

TABLE I-MODES OF A WIND TURBINE UNIT OF A WINDFARM

S. No.	Oscillatory Modes	Freq. (Hz)	Damping Ratio
Mode 1	$-23.17 \pm j491.04$	78.151	4.713 %
Mode 2	$-40.8 \pm j75.587$	12.03	47.49 %
Mode 3	$-8.3 \pm j54.05$	8.602	15.17 %
Mode 4	$-0.52 \pm j3.30$	0.525	15.56 %
Mode 5	$-0.57 \pm j4.93$	0.785	11.48 %
Mode 6	$-0.49 \pm j4.11$	0.654	11.83 %
Mode 7	$-0.0336 \pm j9.096$	**1.448**	**0.369 %**
Mode 8	$-0.0331 \pm j7.322$	**1.165**	**0.452 %**
Mode 9	$-0.0335 \pm j6.102$	**0.971**	**0.548 %**
Mode 10	$-0.0201 \pm j2.009$	**0.318**	**1.001 %**

TABLE II- PARTICIPATION FACTORS OF MODES OF A WIND TURBINE

S. No.	Participating States	Nature	
Mode 1	I_{qsi} (49.2%), I_{dsi} (48.4%)	Electrical	
Mode 2	x_{pli1} (52.2%), θ_{pli} (46.2%)	PLL Mode	
Mode 3	E'_{di} (48.1%),ω_{ri} (43.2%)	Electromechanical	
Mode 4	θ_{twi} (47.5%), ω_{ti} (49.8%) β_i (3.7%)	Mechanical	
Mode 5	$\mathrm{V}_{\mathrm{DC}i}$ (44%),$x_{\mathrm{V}_{\mathrm{DC}}i}$(42.7%)	Control Mode 1	
Mode 6	$x_{\mathrm{P}i}$(43.2%), $x_{I_{dr}i}$(42.7%)	Control Mode 2	
Mode 7	ξ_{i2}(17.4%), $\dot{\xi}_{i2}$(26.6%) ξ_{i3}(21.8%), $\dot{\xi}_{i3}$(31.9%)	Structural Mode 1	Blades
Mode 8	ξ_{i1}(48%), $\dot{\xi}_{i1}$(48.2%)	Structural Mode 2	
Mode 9	ξ_{i2}(32.1%), $\dot{\xi}_{i2}$(23.6%) ξ_{i3}(25.5%), $\dot{\xi}_{i3}$(16.8%)	Structural Mode 3	
Mode 10	ξ_{i4}(49.9%), $\dot{\xi}_{i4}$(50%)	Structural Mode 4: Tower	

TABLE III- INTER AREA MODES (IAMS)

Inter-Area Modes →	IAM 1	IAM 2	IAM 3	IAM 4
Frequency (Hz)	0.39	0.52	0.59	0.78
Damping Ratio	0.46%	1.47%	1.85%	3.35%
Principal Participating States	δ_{15}, ω_{15}, δ_{14}	ω_{16}, δ_{16}, δ_{14}	ω_{13}, δ_{13}, δ_{16}	ω_{15}, δ_{15}, ω_{13}

Authorized licensed use limited to: UNIVERSITY OF SOUTHAMPTON. Downloaded on February 13,2024 at 09:11:53 UTC from IEEE Xplore. Restrictions apply.
© 2023 IEEE. Personal use is permitted, but republication/redistribution requires IEEE permission. See https://www.ieee.org/publications/rights/index.html for more information.

This article has been accepted for publication in IEEE Transactions on Power Systems. This is the author's version which has not been fully edited and content may change prior to final publication. Citation information: DOI 10.1109/TPWRS.2023.3330604

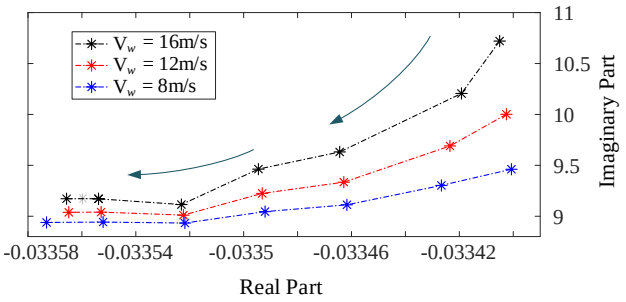

Fig. 6. Structural mode loci when blade specific mass $\sigma_m(l)$ is varied from $0.7-1.3$ in increment of 0.1, with arrow pointing in the variation-direction

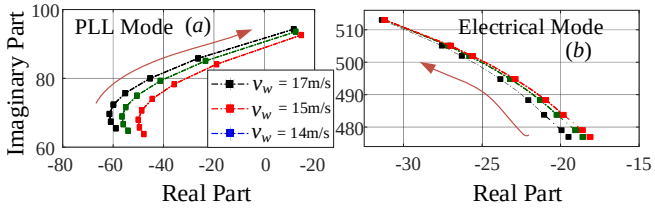

Fig. 7. Eigen-value loci of PLL and electrical modes with the variation of k_{pli1} from $20-100$, with arrows pointing in the direction of increase in k_{pli1}

VI. Case Study

The modified NETS-NYPS 16 machine 68 bus power system with type-3 WTGs based windfarm interconnection at bus number 43 has been used for case study (Fig. 1). The synchronous generators in the test system are represented by a standard IEEE 2.2 subtransient mathematical model. This sixth-order (IEEE 2.2) model is recommended for monitoring and control as per IEEE standards, with two damper coils on q-axis and a field winding and a damper coil on d-axis [38]-[40]. Individual studies are discussed as follows:

A. DAE Model and Eigen Value Analysis

Modal analysis was used to study the nature of the oscillatory modes of the power system with the windfarm. The complete differential-algebraic equation model of the test system with n_s synchronous generators and a windfarm with n_w WTGs is written in a composite form as follows:

B. DAE Model and Eigen Value Analysis

Modal analysis was used to study the nature of the oscillatory modes of the power system with the windfarm. The complete differential-algebraic equation model of the test system with n_s synchronous generators and a windfarm with n_w WTGs is written in a composite form as follows:

$$\dot{\mathbf{X}} = \boldsymbol{f}(\mathbf{X}, \mathbf{Z}, \mathbf{U}) \quad (32)$$

$$\mathbf{0} = \boldsymbol{h}(\mathbf{X}, \mathbf{Z}, \mathbf{U}) \quad (33)$$

$$\mathbf{X} = \left[\mathbf{X}_{s1}\ \mathbf{X}_{s2}\ \dots\ \mathbf{X}_{sn_s}\ \mathbf{X}_{w1}\ \mathbf{X}_{w2}\ \dots\ \mathbf{X}_{wn_w}\right]^{\mathrm{T}}$$

$$\mathbf{Z} = \left[\mathbf{Z}_{s1}\ \mathbf{Z}_{s2}\ \dots\ \mathbf{Z}_{sn_s}\ \mathbf{Z}_{w1}\ \mathbf{Z}_{w2}\ \dots\ \mathbf{Z}_{wn_w}\right]^{\mathrm{T}}$$

$$\mathbf{U} = \left[\mathbf{U}_{s1}\ \mathbf{U}_{s2}\ \dots\ \mathbf{U}_{sn_s}\ \mathbf{U}_{w1}\ \mathbf{U}_{w2}\ \dots\ \mathbf{U}_{wn_w}\right]^{\mathrm{T}}$$

where, $\mathbf{X}_{sj}\ \forall\, j \in \{1, 2, \dots, n_s\}$ and $\mathbf{X}_{wi}\ \forall\, i \in \{1, 2, \dots, n_w\}$ are the state vectors of the j^{th} synchronous machine and i^{th} WTG unit, respectively. $\mathbf{Z}_{sj}\ \forall\, j \in \{1, 2, \dots, n_s\}$ and $\mathbf{Z}_{wi}$ $\forall\, i \in \{1, 2, \dots, n_w\}$ are the algebraic variables of the j^{th} synchronous machine and i^{th} WTG, respectively. Similarly, $\mathbf{U}_{sj}\ \forall\, j \in \{1, 2, \dots, n_s\}$ and $\mathbf{U}_{wi}\ \forall\, i \in \{1, 2, \dots, n_w\}$ are the inputs of the j^{th} synchronous machine and i^{th} type-3 wind-turbine, respectively. The description of the state, algebraic and input vectors for a synchronous machine is detailed in [40], while for WTG unit these vectors are defined below.

$$\mathbf{X}_{wi}^{\mathrm{T}} = [E'_{qi}\ E'_{di}\ I_{qsi}\ I_{dsi}\ \omega_{ti}\ \theta_{twi}\ \omega_{ri}\ \mathrm{V}_{\mathrm{DC}i}\ x_{\mathrm{P}i}\ x_{\mathrm{Q}i}\ x_{\mathrm{I}_{dr}i}\ \beta_i\ \theta_{bi}\ x_{\mathrm{I}_{qr}i}\ x_{\mathrm{V}_{\mathrm{DC}}i}\ x_{\mathrm{Q}_{\mathrm{GSC}}i}\ x_{pli1}\ x_{pli2}\ \theta_{pli}\ \xi_{i1}\ \xi_{i2}\ \xi_{i3}\ \xi_{i4}\ \dot{\xi}_{i1}\ \dot{\xi}_{i2}\ \dot{\xi}_{i3}\ \dot{\xi}_{i4}] \quad (34)$$

$$\mathbf{Z}_{wi}^{\mathrm{T}} = [\mathrm{V}_{qsi}\ \mathrm{V}_{dsi}\ \mathrm{V}_{qgi}\ \mathrm{V}_{dgi}\ \mathrm{V}_{qri}\mathrm{V}_{dri}],\ \mathbf{U}_{wi} = [v_w\ \mathrm{V}_{pcw}\ \gamma_{pcw}] \quad (35)$$

Upon linearization of equations (32)-(33) at an equilibrium point $(\mathbf{X_0}, \mathbf{Z_0}, \mathbf{U_0})$ the system matrix $\mathbf{A_s}$ is obtained as.

$$\mathbf{A_s} = \partial \boldsymbol{f}/\partial \mathbf{X} - (\partial \boldsymbol{f}/\partial \mathbf{Z})(\partial \boldsymbol{h}/\partial \mathbf{Z})^{-1}(\partial \boldsymbol{h}/\partial \mathbf{X}) \quad (36)$$

The eigenvalues of the power system with $n_s = 16$ and $n_w = 50$ (i.e., 16 synchronous machines and 50 WTGs in the wind farm) are plotted in Fig. 5. As an example, the oscillatory modes in which the states of the 3^{rd} turbine unit participate have been tabulated in Table-I, along with the principle participating states in Table-II. Participation factor analysis was used to identify the participation of machines states including windfarm WTG states in the modes [40]. The principal states which participate in the inter-area modes of the test system are given in Table-III. It can be deduced that windfarm states participation in the power system inter-area modes is marginal and the modes in which windfarm states participate are generally *local*. The impact of parameter variations (specific mass, and PLL parameters) on these local oscillatory modes are investigated next.

C. Parameter Variations and Windfarm Oscillatory Modes

The specific variation of a mode with a variation in the wind turbine parameters is described as follows:

1) Specific mass of the turbine blades and structural modes:

Blade structural modes (Mode 7-9 in Table-I-II) are sensitive to the variation in the specific mass of the blades. The impact of variation in the specific mass of the blades has minimal or no impact on other oscillatory modes. The sensitivity of the structural modes to system parameter variation was studied by varying the specific mass of the blades ($0.7 \le \sigma_m(l) \le 1.3$). For three different wind speeds, the corresponding loci of the structural mode (Mode 7) were plotted as shown in Fig. 6. For a given wind speed, the frequency of these structural modes (Mode 7-9) decreases with increase in specific mass while the damping ratio remains almost unaffected (Fig. 6).

2) Variation in synchronization loop (PLL) parameters:

The stability margins in the case of type-3 WTG systems reduce when its interconnection impedance is relatively large and it is operated in super-synchronous speed range [7], [9]. Under such a condition, the impact of variation in the PLL parameter (k_{pli1}) on the oscillatory modes of the 3^{rd} unit of the windfarm is presented. The PLL mode gets affected upon the variation in the k_{pli1} ($20 \le k_{pli1} \le 100$) and it can become unstable for large variations (Fig. 7 (a)). The effect on the electrical mode is marginal (Fig. 7 (b)). The impact of other parameters on the windfarm oscillatory modes has been investigated in detail in [7], [9], [15], [48] and the results are in agreement. It is noted that the structural modes (not shown here due to limited space) are least sensitive to the grid strength or PLL parameters variations.

D. Nonlinear time-domain analysis

The simulations of the test system have been performed

Authorized licensed use limited to: UNIVERSITY OF SOUTHAMPTON. Downloaded on February 13,2024 at 09:11:53 UTC from IEEE Xplore. Restrictions apply.
© 2023 IEEE. Personal use is permitted, but republication/redistribution requires IEEE permission. See https://www.ieee.org/publications/rights/index.html for more information.

This article has been accepted for publication in IEEE Transactions on Power Systems. This is the author's version which has not been fully edited and content may change prior to final publication. Citation information: DOI 10.1109/TPWRS.2023.3330604

in MATLAB using ode15s solver on a personal desktop with $i7$-9750H CPU @ 2.6 GHz and 7.85 GB usable RAM. To study the impact of gear backlash, nonlinear time-domain simulations were performed (Fig. 8). Fourier series analysis of the time response was used to corroborate the findings of the linear analysis (Section-V-A-B). The following three studies were undertaken to study the impact of the backlash on the dynamic performance of the wind turbines:

1) Step change in wind speed:

The test system was initialized at its operating point with individual units of the windfarm operating at different wind speeds. Each unit was subjected to a change in wind speed from $v_w\ (ms^{-1})$ to $0.5v_w\ (ms^{-1})$ for two seconds, at $t = 10s$. Due to this change in wind speed, there was an instantaneous imbalance between input mechanical and output electrical powers, resulting in the deceleration of the rotors for two seconds. At $t = 12s$, when the wind speed was restored back to its nominal value, the rotors accelerated again till rotor speeds of the WTG units stabilized. The corresponding net electrical power output of the windfarm with and without gear backlash is shown in Fig. 8. The corresponding time evolution in the rotor speeds of the DFIG units operating in super-synchronous ($v_w = 17ms^{-1}$) and sub-synchronous speed ranges ($v_w = 8ms^{-1}$) are, respectively, shown in Fig. 9 (*a-b*).

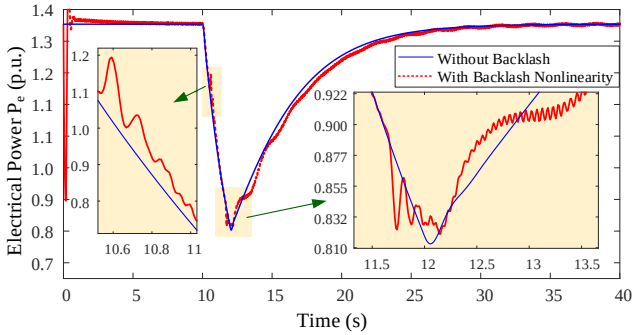

Fig. 8. Net windfarm output power in $p.u.$, when wind speed of the individual turbine units changes by 50% at $t = 10s$ for two seconds.

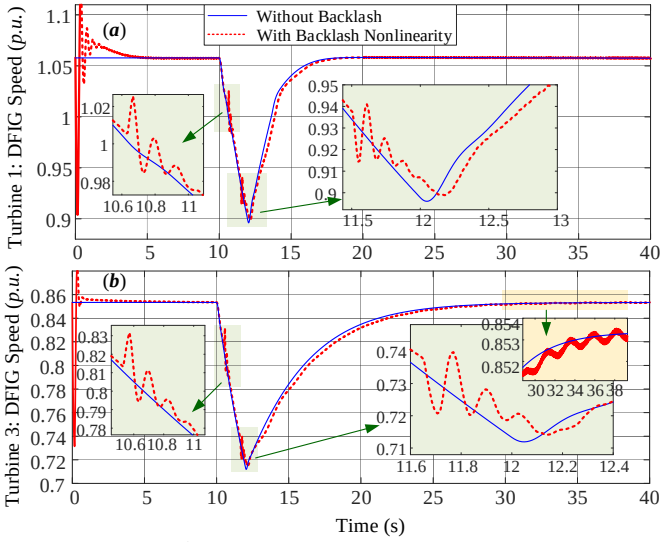

Fig. 9. Rotor speeds of the DFIGs operating in (*a*) super-synchronous speed range and (*b*) sub-synchronous speed range when wind speed changes by 50% for two seconds.

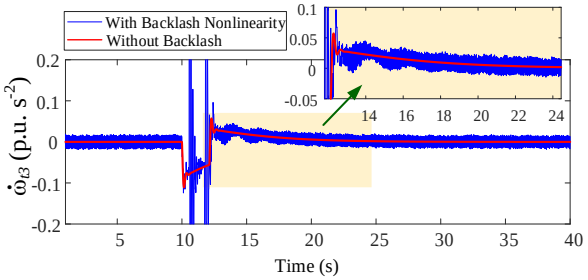

Fig. 10. Turbine acceleration of the DFIG unit operating in sub-synchronous speed range when wind speed changes by 50% for two seconds.

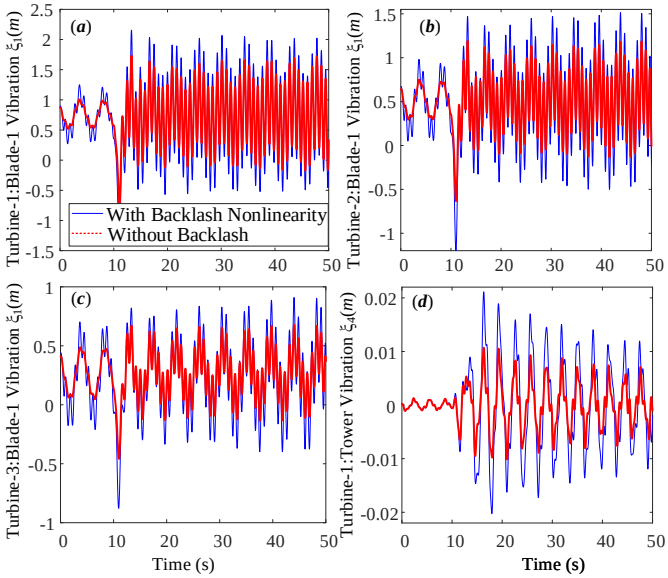

Fig. 11: Case Study C1: Vibrations in the turbine blades and tower-top.

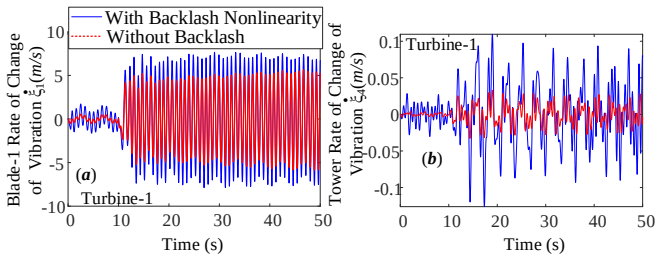

Fig. 12: Case Study C1: Turbine and tower-top vibration acceleration (m/s).

The backlash effect stimulates the electro-mechanical mode (8.602 Hz: Mode-3) and it introduces a lag in the time response (Fig. 8-Fig. 9) which has implications on the design approach of auxiliary damping controllers [9]. The turbine acceleration of the unit operating in a sub-synchronous speed range ($v_w = 8ms^{-1}$) is shown in Fig. 10. It is clear from Fig. 10 that the backlash has a more pronounced effect on the turbine acceleration which translates into an equivalent tangential force (36). This induces edgewise/lateral vibrations in the turbine blades and its tower structure. For three units of the windfarm, with input wind speeds as $16ms^{-1}$ (high speed), $12ms^{-1}$ (medium speed) and $8ms^{-1}$ (low speed), respectively, the edgewise blade vibrations of these three units, for the same disturbance scenario, are shown in Fig. 11 (*a-c*). The vibration in the tower-top of the unit with $v_w = 16ms^{-1}$ is shown in Fig. 11 (*d*). The corresponding acceleration in the edgewise and tower-top vibrations of the same unit has been plotted in Fig. 12.

Authorized licensed use limited to: UNIVERSITY OF SOUTHAMPTON. Downloaded on February 13,2024 at 09:11:53 UTC from IEEE Xplore. Restrictions apply.
© 2023 IEEE. Personal use is permitted, but republication/redistribution requires IEEE permission. See https://www.ieee.org/publications/rights/index.html for more information.

This article has been accepted for publication in IEEE Transactions on Power Systems. This is the author's version which has not been fully edited and content may change prior to final publication. Citation information: DOI 10.1109/TPWRS.2023.3330604

TABLE IV-PERFORMANCE INDEX $\mathcal{J}_{b1}$

Δv_w	Index	$v_w = 16m/s$	$v_w = 12m/s$	$v_w = 8m/s$
10%	$\mathcal{J}_{b1} \rightarrow$	0.232	0.221	0.219
30%	$\mathcal{J}_{b1} \rightarrow$	0.471	0.438	0.422
50%	$\mathcal{J}_{b1} \rightarrow$	0.926	0.897	0.869

TABLE V-PERFORMANCE INDEX $\mathcal{J}_{b2}$

ϱ_i	$\Delta v_w \rightarrow$	20%	30%	40%	50%	60%
0.050	$\mathcal{J}_{b2} \rightarrow$	0.046	0.079	0.898	0.122	0.159
0.075	$\mathcal{J}_{b2} \rightarrow$	0.047	0.082	0.955	0.142	0.196
0.100	$\mathcal{J}_{b2} \rightarrow$	0.051	0.087	0.110	0.198	0.272

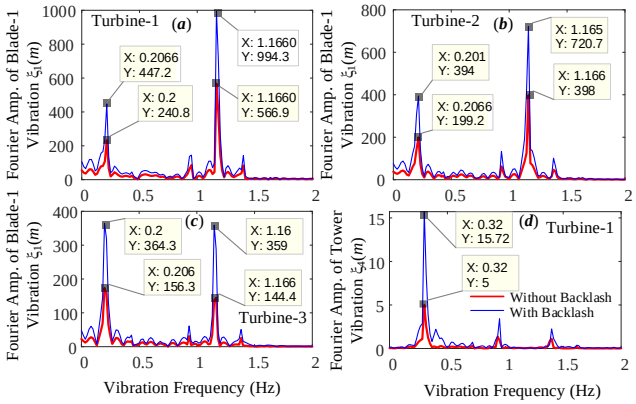

Fig. 13: Case Study C1: Fourier analysis of the vibrations.

The impact of backlash width on the blade and tower-top vibration amplifications were quantified using the index $\mathcal{J}_{b1}$:

$$\mathcal{J}_{b1} = \left(\xi_{ij,w}^{max} - \xi_{ij,wo}^{max}\right)/\xi_{ij,wo}^{max} \qquad (37)$$

where, $\xi_{ij,w}^{max}$ and $\xi_{ij,wo}^{max}$ are the maximum edgewise vibrations in the j^{th} blade of the i^{th} turbine of a windfarm with and without backlash, respectively. It represents the amplification of blade vibrations due to backlash as a fraction of maximum blade vibrations when the backlash effect is completely ignored. Index $\mathcal{J}_{b1}$ has been tabulated in Table-IV which illustrates the aggravating impact of backlash on the blade vibrations for different percentage changes in the wind speed.

A higher value of index implies more aggravating impact. Likewise, an index $\mathcal{J}_{b2}$ defined by (38) examines the overall impact of backlash nonlinearity on the windfarm dynamics.

$$\mathcal{J}_{b2} = \int_{t1}^{t2}\left(\left|\mathrm{P}_w^{wf}(t) - \mathrm{P}_{wo}^{wf}(t)\right|\right)dt \qquad (38)$$

where, $\mathrm{P}_w^{wf}(t)$ and $\mathrm{P}_{wo}^{wf}(t)$ are, respectively, the net power output from the windfarm with and without backlash. This index "$\mathcal{J}_{b2}$" is similar to "integral absolute error (IAE)" used in the literature to quantify the difference between reference and output trajectories. For different percentage wind speed changes and backlash widths, $\mathcal{J}_{b2}$ has been tabulated in Table-V illustrating the impact of the backlash. A higher value of index implies more aggravating impact.

Furthermore, the Fourier transform of the time response with a window size of $40s$ was used to determine the frequency of these oscillations in the edgewise vibrations. The corresponding Fourier amplitude versus vibration frequency plots are shown in Fig. 13 for illustration. There are two dominant frequency components in the edgewise vibrations: $0.21\,Hz$ and $1.165\,Hz$. The $0.21\,Hz$ corresponds to blade rotor rotation at 12.1 revolutions-per-minute with respect to structure supporting the rotor, whereas $1.165\,Hz$ is the modal frequency of Mode-8 given in Table-I and Table-II in which structural states of the Blade-1 participate. The dominant frequency ($0.32\,Hz$) in the tower-top vibration is the modal frequency of Mode-10 given in Table-I and Table-II in which structural states of the tower structure participate. Therefore, the Fourier analysis of the time domain response supports the findings via linear analysis.

2) Varying wind speed:

To study the impact of wind variability on the windfarm dynamic performance with/without the gear backlash, the Van'der Hoven wind spectrum (Fig. 4) of Section-III was used to simulate the wind speeds for individual turbine units. Due to this varying wind speed, there was an instantaneous imbalance between input mechanical and output electrical powers. The corresponding time evolution in the rotor speeds of the DFIG units operating in super-synchronous and sub-synchronous speed range are, respectively, shown in Fig. 14 (*a*-*b*). There is a lag in the time-response and stimulation of electromechanical mode, illustrating the impact of backlash. Similar to the aforementioned case study, the edgewise blade vibration of the units operating at different wind speeds are shown in Fig. 15. The corresponding acceleration in the blade and tower-top vibrations of the turbine operating at a relatively higher wind speed is shown in Fig. 16. With backlash, the acceleration is large, illustrating the aggravating impact due to gear backlash. The impact is proportional to the variability in the wind speed, i.e. higher the variability, more is the impact of the backlash. The difference between the net power output from the windfarm with and without the gear backlash is shown in Fig. 17 (*a*), illustrating its impact on the overall windfarm dynamics. The Fourier analysis of the time response of structural states for a wind turbine operating at relatively higher wind speed is depicted and illustrated in Fig. 17 (*b*). The dominant frequency ($1.167Hz$) component in the blade vibrations is approximately same as modal frequency of the structural mode (Mode-8 in Table-I and Table-II) thereby validating the linear analysis findings.

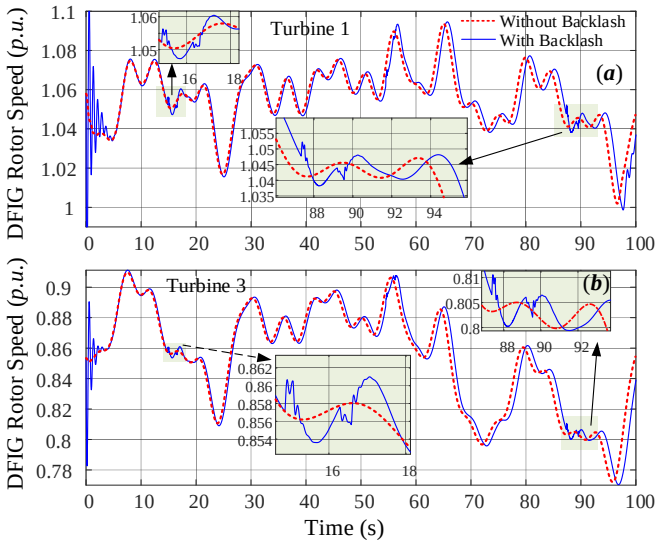

Fig. 14. Rotor speeds of the DFIGs operating in (*a*) super-synchronous speed range and (*b*) sub-synchronous speed range under dynamic wind conditions.

Authorized licensed use limited to: UNIVERSITY OF SOUTHAMPTON. Downloaded on February 13,2024 at 09:11:53 UTC from IEEE Xplore. Restrictions apply.
© 2023 IEEE. Personal use is permitted, but republication/redistribution requires IEEE permission. See https://www.ieee.org/publications/rights/index.html for more information.

This article has been accepted for publication in IEEE Transactions on Power Systems. This is the author's version which has not been fully edited and content may change prior to final publication. Citation information: DOI 10.1109/TPWRS.2023.3330604

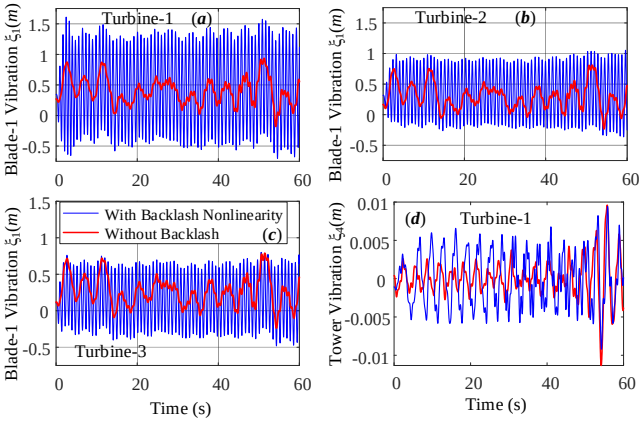

Fig. 15: Case Study C2, dynamic wind case: Blade and tower-top vibrations

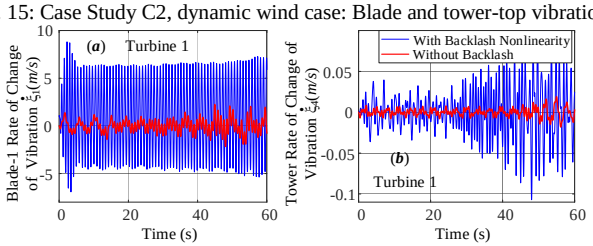

Fig. 16: Case Study C2: Dynamic wind conditions: Blade-1 and tower-top vibration acceleration (m/s) of the unit operating at higher wind speed.

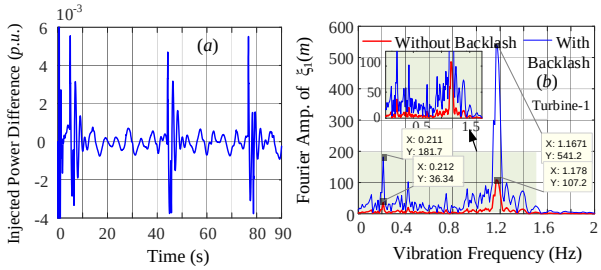

Fig. 17: Case Study C2: (*a*) $P_w^{wf}(t) - P_{wo}^{wf}(t)$, (*b*) Fourier analysis of the vibrations in Blade-1.

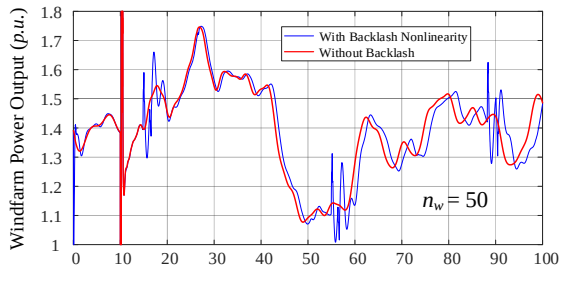

Fig. 18: Case Study C3: Windfarm power output with/without backlash following a network disturbance.

3) Variable wind speed and a network disturbance:

In this case study, the test system (Fig. 1) was subjected to a three-phase fault near bus number 43 and clearing the fault after $200ms$ to simulate a network disturbance. The rotors of the wind turbine units accelerate due to the resultant imbalance between electrical and mechanical powers. The net electrical power output of the windfarm with and without backlash is shown in Fig. 18. The rotor speeds of the two wind turbine units operating in super-synchronous and sub-synchronous speed ranges are respectively shown in Fig. 19 (*a*-*b*). Similar to Case Study-1, the gear backlash stimulates the electro-mechanical mode (8.602 Hz: Mode-3) and there is a lag in the time responses (Fig. 19). The turbine acceleration manifests itself as an aggravating force on the wind-turbine structure and it amplifies the vibrations in its blades and the tower-top. The resultant edgewise vibrations in Blade-1 of the two units operating at different wind speeds are shown in Fig. 20 (*a*-*b*).

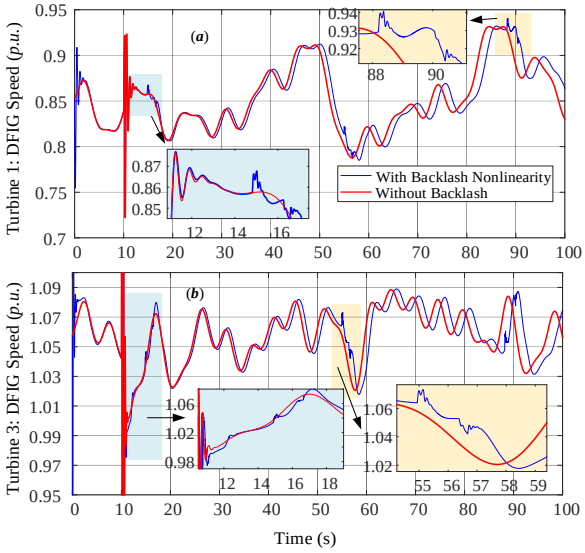

Fig. 19. Rotor speeds of the DFIGs operating in (*a*) super-synchronous range and (*b*) sub-synchronous range under dynamic wind conditions and a network disturbance.

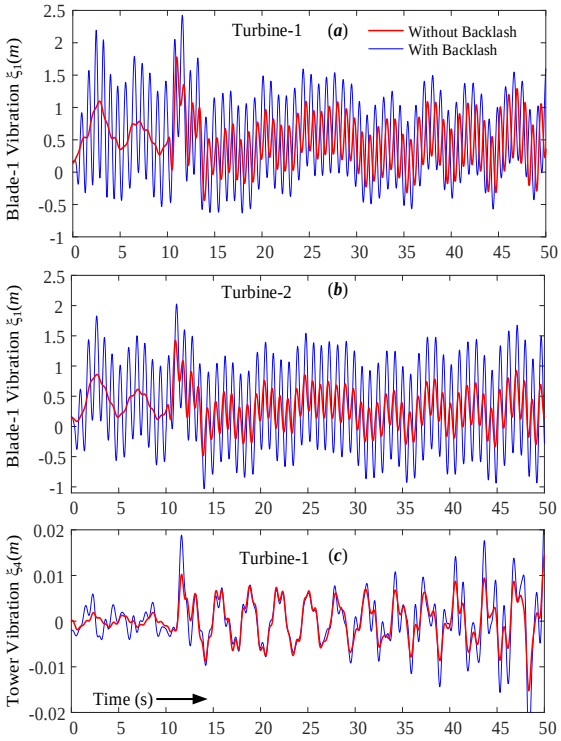

Fig. 20: Case Study C3, Dynamic wind conditions and a network disturbance: Vibrations in Blade-1 and tower-top.

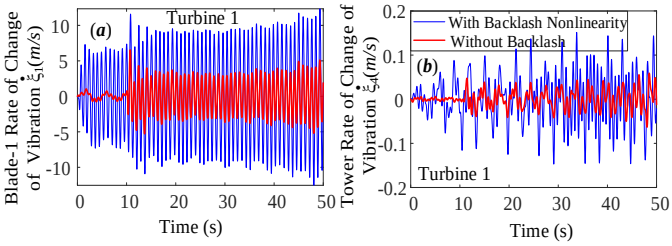

Fig. 21: Case Study C3, Dynamic wind conditions and a network disturbance: Blade-1 and tower-top vibration acceleration (m/s) of the unit operating at higher wind speed.

Authorized licensed use limited to: UNIVERSITY OF SOUTHAMPTON. Downloaded on February 13,2024 at 09:11:53 UTC from IEEE Xplore. Restrictions apply.
© 2023 IEEE. Personal use is permitted, but republication/redistribution requires IEEE permission. See https://www.ieee.org/publications/rights/index.html for more information.

This article has been accepted for publication in IEEE Transactions on Power Systems. This is the author's version which has not been fully edited and content may change prior to final publication. Citation information: DOI 10.1109/TPWRS.2023.3330604

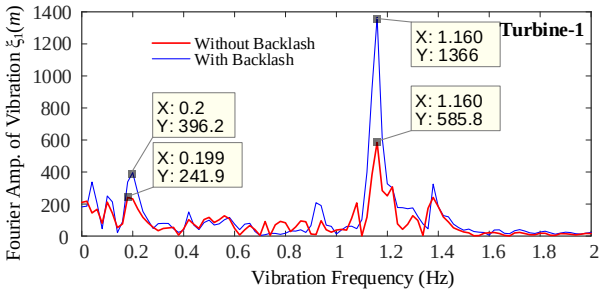

Fig. 22: Case Study C3: Fourier analysis of the vibrations in Blade-1.

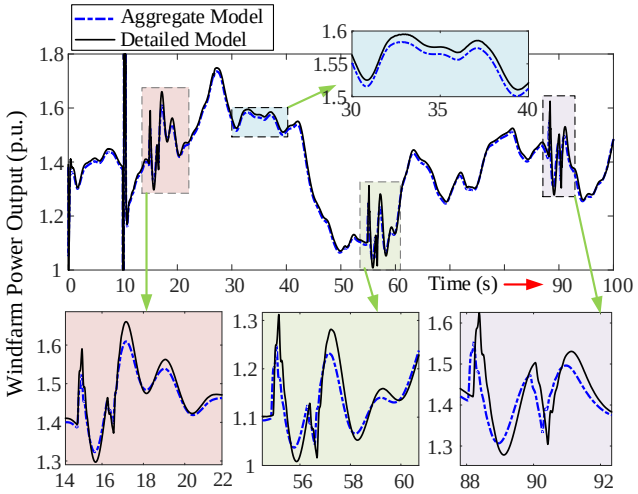

Fig. 23: Windfarm power output with detailed and aggregate models.

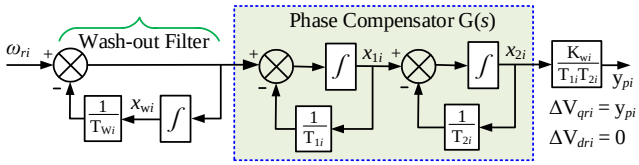

Fig. 24: Auxiliary power system stabilizer (PSS).

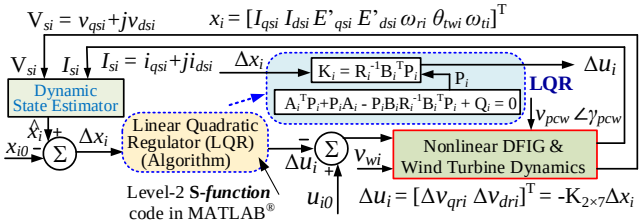

Fig. 25: LQR based damping controller for DFIG-WTGs

The vibrations in the tower-top of the unit operating in the super-synchronous speed range is shown in Fig. 20 (*c*). The corresponding vibration accelerations are shown in Fig. 21. With backlash, the impact on vibrations is more pronounced. Similar to the previous case study, the Fourier analysis of the vibrations in Blade-1 of the wind-turbine unit operating at a relatively higher wind speed was performed (Fig. 22). The dominant frequency ($1.16Hz$) component in the vibrations in Blade-1 of this unit is approximately same as the modal frequency of the structural mode (Mode-8 in Table-I and Table-II) thereby validating the linear analysis findings.

E. Aggregate vs Detailed Model

The aggregation approaches for DFIG-WTG based power systems have some limitations and exclude some critical aspects in the modeling. Besides many simplifications the aggregation approaches [35]-[36] based on parametric scaling assume that incident wind velocities and interconnecting impedances are equal. The impact of these inadequacies in the aggregate modeling approach in comparison to the detailed modeling approach introduced here has been illustrated. The test system (Fig. 1) was subjected to a three-phase fault near bus number 43 and the fault was cleared after $200ms$. The net electrical power output of the windfarm with aggregated model [35]and with detailed model is shown in Fig. 23. It can be observed that the response of the aggregate model does not match the response of the detailed model due to modeling assumptions.

TABLE VI-MODES OF A WTG UNIT OF A WINDFARM (WITH PSS)

S. No.	Oscillatory Modes	Freq. (Hz)	Damping Ratio
Mode 1	$-24.38 \pm j487.01$	77.51	5.01 %
Mode 2	$-42.75 \pm j75.398$	12.00	49.32 %
Mode 3	$-11.67 \pm j52.27$	8.319	21.8 %
Mode 4	$-1.079 \pm j3.173$	0.504	32.2 %
Mode 5	$-0.962 \pm j4.875$	0.776	19.35 %
Mode 6	$-0.842 \pm j4.084$	0.650	20.2 %
Mode 7	$-0.0337 \pm j9.101$	**1.448**	**0.370 %**
Mode 8	$-0.0331 \pm j7.322$	**1.165**	**0.452 %**
Mode 9	$-0.0335 \pm j6.102$	**0.971**	**0.548 %**
Mode 10	$-0.0202 \pm j2.00$	**0.318**	**1.001 %**

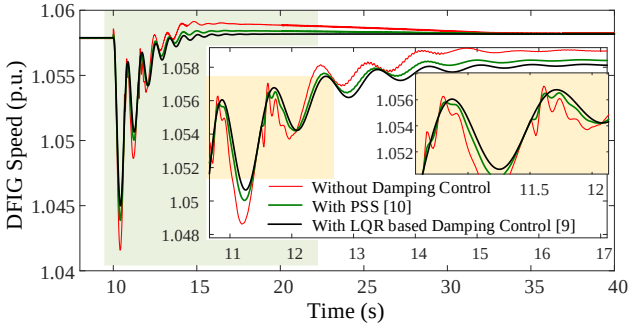

Fig. 26: Impact of damping control considering backlash nonlinearity.

VII. IMPACT OF AUXILIARY DAMPING CONTROL

Auxiliary damping controllers [9], [15] based on simplistic models of type-3 WTGs were used for suppression of local electromechanical oscillations considering backlash. The impact of damping controllers on the oscillation suppression is discussed below.

A. Power System Stabilizer [10], [15]

Phase compensation-based power system stabilizer (PSS) consists of a washout filter block, a stabilizer gain and a lead-lag compensator (Fig. 24). In this damping controller paradigm, DFIG rotor speed (ω_{ri}) acts as an input for the PSS to modulate V_{qri}, thereby modulating the developed torque. The dynamical equations of PSS for its integration with the DFIG-WTG dynamics are written as follows:

$$\dot{x}_{wi} = \omega_{ri} - T_{Wi}^{-1} x_{wi} \quad (39)$$

$$\dot{x}_{1i} = \omega_{ri} - T_{Wi}^{-1} x_{wi} - T_{1i}^{-1} x_{1i} \quad (40)$$

$$\dot{x}_{2i} = x_{1i} - T_{2i}^{-1} x_{2i} \quad (41)$$

$$y_{pi} = K_{Wi} x_{2i} / T_{1i} T_{2i} \quad (42)$$

where, T_{wi} is the washout filter time constant, K_{Wi} is the stabilizer gain, T_{1i} and T_{2i} are the compensator stage time constants and $y_{pi} = \Delta V_{qri}$ [10]. x_{wi}, x_{1i} and x_{2i} are the washout filter and compensator stage state variables, respectively.

Authorized licensed use limited to: UNIVERSITY OF SOUTHAMPTON. Downloaded on February 13,2024 at 09:11:53 UTC from IEEE Xplore. Restrictions apply.
© 2023 IEEE. Personal use is permitted, but republication/redistribution requires IEEE permission. See https://www.ieee.org/publications/rights/index.html for more information.

This article has been accepted for publication in IEEE Transactions on Power Systems. This is the author's version which has not been fully edited and content may change prior to final publication. Citation information: DOI 10.1109/TPWRS.2023.3330604

TABLE VII-MODES OF WTG UNIT OF A WINDFARM (WITH LQR)

S. No.	Oscillatory Modes	Freq. (Hz)	Damping Ratio
Mode 1	$-24.3 \pm j485.44$	77.26	5.00 %
Mode 2	$-39.7 \pm j74.769$	11.90	49.58 %
Mode 3	$-15.42 \pm j51.53$	8.201	28.66 %
Mode 4	$-1.625 \pm j3.078$	0.490	46.69 %
Mode 5	$-1.3245 \pm j4.80$	0.764	26.60 %
Mode 6	$-1.133 \pm j4.071$	0.648	26.81 %
Mode 7	$-0.0337 \pm j9.100$	**1.448**	**0.370 %**
Mode 8	$-0.0331 \pm j7.322$	**1.165**	**0.452 %**
Mode 9	$-0.0335 \pm j6.102$	**0.971**	**0.548 %**
Mode 10	$-0.0203 \pm j2.00$	**0.318**	**1.001 %**

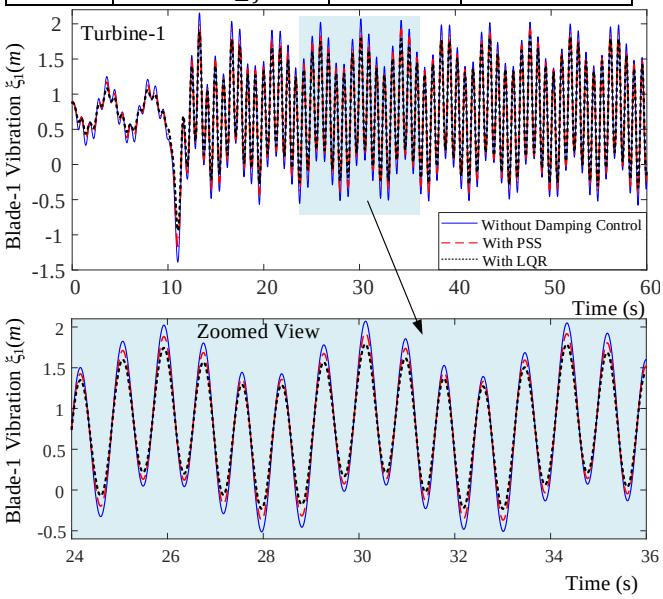

Fig. 27: Impact of traditional damping control on blade vibrations.

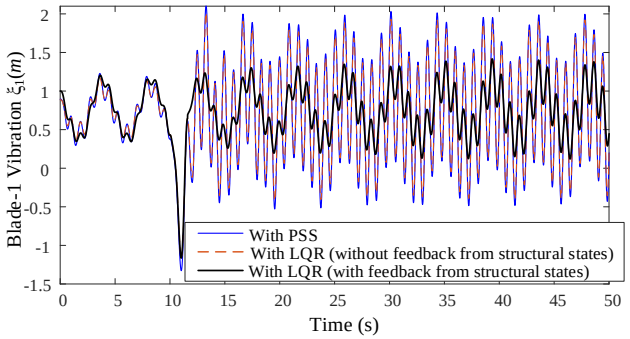

Fig. 28: Impact of damping control (with structural states in the feedback) on blade vibrations.

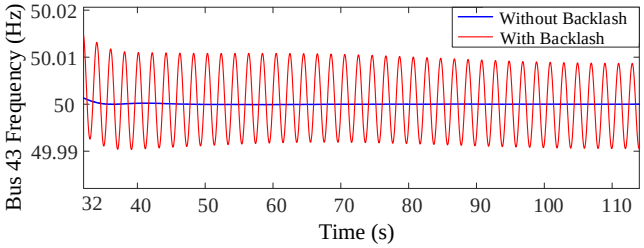

Fig. 29: Bus frequency at the point of interconnection of windfarm.

B. *Damping Control based on Linear Quadratic Regulator* (LQR):

In this auxiliary controller, V_{qri} and V_{dri} were modulated to control the electrical torque to improve the damping performance using estimated electromechanical states ($I_{qsi}\ I_{dsi}\ E'_{qi}\ E'_{di}\ \omega_{ri}\ \theta_{twi}\ \omega_{ti}$) as inputs (Fig. 25). This design is based on an optimal control methodology wherein the control effort (ΔV_{qri}, ΔV_{dri}) is derived by the minimization of the cost-functional J^i_{LQR} (43).

$$J^i_{LQR} = \int_0^\infty (\Delta x_i^T Q_i \Delta x_i + \Delta u_i^T R_i \Delta u_i)\, dt \qquad (43)$$

where Q_i and R_i are the weighted positive definite matrices of appropriate dimensions for an i^{th} WTG unit. Accordingly, the optimal control law is given by (44).

$$\Delta u_i = -K_i \Delta x_i = -R_i^{-1} B_i^T P_i \Delta x_i \qquad (44)$$

where, P_i is the obtained by solving the algebraic Ricaati equation given by (45).

$$A_i^T P_i + P_i A_i - P_i B_i R_i^{-1} B_i^T P_i + Q_i = 0 \qquad (45)$$

where, A_i and B_i are the linearized matrices of the i^{th} WTG unit dynamics.

To study and explore the impact of damping controllers on the oscillation suppression, each wind turbine unit of the wind farm was subjected to an input wind speed change (from v_w to $0.3v_w$) at $t = 10s$ for one second. The rotor speed of a DFIG-WTG unit operating in super-synchronous speed range with and without the aforementioned damping controllers is shown in Fig. 26, while the Blade-1 edgewise vibration of the corresponding turbine is shown in Fig. 27. These controllers improve the damping of low-frequency electromechanical/mechanical modes significantly whereas the damping of structural modes improves marginally. For illustration the oscillatory modes in which the states of the 3^{rd} WTG unit participate with PSS and with LQR have been tabulated in Table-VI and Table-VII, respectively.

The suppression of vibrations can be enhanced by using structural states in the auxiliary feedback controller design. The design of such controller requires consideration of structural states ($\xi_{i1}\ \xi_{i2}\ \xi_{i3}\ \xi_{i4}\ \dot{\xi}_{i1}\ \dot{\xi}_{i2}\ \dot{\xi}_{i3}\ \dot{\xi}_{i4}$) for use in the control of active tendons, which produces inhibiting forces to damp out the induced vibrations in the turbine structure. Using structural states in the feedback damping controller [9] offers significantly superior performance in suppressing the vibrations compared to traditional damping controllers as illustrated in Fig. 28.

VIII. FREQUENCY STABILITY AND BACKLASH

The impact of backlash nonlinearity on the frequency stability of the system has also been studied. Increased penetration of power from DFIG based WTGs necessitates it to participate in the frequency regulation of the power system [3]. Gear backlash in the drive train of the WTGs tends to produce sustained oscillations in the system frequency. The effect is similar to the impact of governor nonlinearities (dead-band) in the traditional synchronous generators [49].

The frequency at Bus 43 of the test system following a wind perturbation is shown in Fig. 29. The backlash nonlinearity induced sustained oscillations in the frequency can have potential implications on the frequency stability of the system. Therefore, the performance of auxiliary frequency controllers may not be adequate if backlash/dead-band effects are not compensated and addressed in the controller design.

IX. DISCUSSIONS

Based on the case studies, the following discussion points are presented:

Authorized licensed use limited to: UNIVERSITY OF SOUTHAMPTON. Downloaded on February 13,2024 at 09:11:53 UTC from IEEE Xplore. Restrictions apply.
© 2023 IEEE. Personal use is permitted, but republication/redistribution requires IEEE permission. See https://www.ieee.org/publications/rights/index.html for more information.

This article has been accepted for publication in IEEE Transactions on Power Systems. This is the author's version which has not been fully edited and content may change prior to final publication. Citation information: DOI 10.1109/TPWRS.2023.3330604

1. Based on linear analysis, it can be inferred that the structural modes (Mode-7-Mode-10 in Table-I) are sensitive to the variation in the specific mass of turbine blades and are almost insensitive to the variation in other parameters of the wind turbine. The electrical mode (Mode-1) and the PLL mode (Mode-2) are sensitive to the variations in the PLL parameters whereas structural, mechanical and electromechanical modes remain unaffected (Mode-3-Mode-10). Also, all the modes associated with the windfarm are local in nature.
2. The effect of backlash nonlinearity is not captured accurately in linear analysis. Nonlinear time domain simulations appropriately capture the effect of backlash dead-zone. Therefore, in the event of any significant network disturbance and/or wind speed change, nonlinear time domain simulations with detailed model must be used to study and explore the dynamic performance of the system.
3. Turbine acceleration due to sudden changes in wind speed and/or network disturbance leads to amplification of blade and tower-top vibrations. With gear backlash, the effect is highly pronounced. More severe the disturbance, more pronounced is the backlash effect. Two novel indices are proposed to measure the effect of these disturbance and backlash width on the blade vibrations.
4. Backlash induces and amplifies the electromechanical oscillation mode (Mode-3) and causes lag in the time evolution of the windfarm electromechanical states. Thus, the current practice of ignoring the effect of backlash during controller design may not guarantee adequate performance.
5. Structural states predominantly participate in the structural modes. The conventional damping controllers have a marginal impact on the suppression of corresponding vibrations from structural modes. Therefore, the amplifications in the blade vibrations can be controlled and mitigated by designing active dampers which use estimated structural states (otherwise unmeasurable) as inputs. The superiority of feedback controllers (with feedback from high participating states) in the effective control of oscillatory dynamics has been well established in the literature [9], [40].
6. Backlash in the drivetrain has an adverse impact on the frequency stability of the system. Therefore, its effect must be considered during the design of auxiliary controllers to guarantee the adequate performance.

X. Conclusions and the Future Study

A model of a windfarm comprising of type-3 WTGs considering detailed structural and electromechanical dynamics including gear backlash nonlinearity has been introduced to study system dynamics in a multimachine environment. Linear analysis was used to study the nature of various modes pertaining to windfarm and the sensitivity of these modes to the variation in the different system parameters. Time-domain simulations were used to study the impact of backlash nonlinearity on oscillatory behaviour which otherwise may not be captured in linear analysis. It has been shown that backlash nonlinearity has an aggravating impact, and it causes amplification of turbine blade vibrations. The eigenvalue analysis findings were complemented by Fourier analysis of the time response. Realistic stochastic wind speed profile (modelled using the Van'der Hoven spectrum) was also used to evaluate the dynamic performance of the windfarm with type-3 WTGs. It has been found that traditional damping controllers are not effective in arresting the amplified blade vibrations due to structural modes. This necessitates the use of auxiliary active dampers considering structural states in the control design. The design of such a controller can be based on prior estimation of the structural states, and using them to generate a feedback control signal. Studying the impact of auxiliary pitch angle controller can also be a subject of future study. Additionally, fast blade vibrations and system nonlinearities from gear backlash may qualitatively/quantitatively influence the fast frequency and inertial responses [23]-[24] of the type-3 WTGs. It is recommended to study the overall dynamics including this impact in detail using the complete model investigated in this paper wherein both the mechanical and electrical dynamics have been modelled in detail unlike traditional approaches.

Appendix-A

Electrical Dynamics [7]

$$\omega_{si}^{-1}\omega_{\mathrm{B}}^{-1}\dot{E}'_{qi} = R_{2i}I_{dsi} - \omega_{si}^{-1}T_{ri}^{-1}E'_{qi} + (1-\omega_{si}^{-1}\omega_{ri})E'_{di} - k_{mi}\mathrm{V}_{dri} \quad \text{(A1)}$$

$$\omega_{si}^{-1}\omega_{\mathrm{B}}^{-1}\dot{E}'_{di} = -R_{2i}I_{qsi} - \omega_{si}^{-1}T_{ri}^{-1}E'_{di} - (1-\omega_{si}^{-1}\omega_{ri})E'_{qi} + k_{mi}\mathrm{V}_{qri} \quad \text{(A2)}$$

$$k_i\dot{I}_{qsi} = -R_{1i}I_{qsi} + \omega_{si}L'_{si}I_{dsi} + \omega_{si}^{-1}\omega_{ri}E'_{qi} - \omega_{si}^{-1}T_{ri}^{-1}E'_{di} - \mathrm{V}_{qsi} + k_{mi}\mathrm{V}_{qri} \quad \text{(A3)}$$

$$k_i\dot{I}_{dsi} = -R_{1i}I_{dsi} - \omega_{si}L'_{si}I_{qsi} + \omega_{si}^{-1}\omega_{ri}E'_{di} + \omega_{si}^{-1}T_{ri}^{-1}E'_{qi} - \mathrm{V}_{dsi} + k_{mi}\mathrm{V}_{dri} \quad \text{(A4)}$$

$$I_{qri} = -\omega_s^{-1}L_{mi}^{-1}E'_{di} - k_{mi}I_{qsi} \quad \text{(A5)}$$

$$I_{dri} = \omega_s^{-1}L_{mi}^{-1}E'_{qi} - k_{mi}I_{dsi} \quad \text{(A6)}$$

$$\mathrm{C}_i\mathrm{V}_{\mathrm{DC}i}\dot{\mathrm{V}}_{\mathrm{DC}i} = V_{dri}I_{dri} + V_{qri}I_{qri} - V_{dgi}I_{dgi} - V_{qgi}I_{qgi} \quad \text{(A7)}$$

where, $k_i = L'_{si}/\omega_{e\mathrm{B}}$, $R_{1i} = R_{2i} + R_{si}$, $R_{2i} = k_{mi}^2R_{ri}$, $k_{mi} = L_{mi}/L_{ri}$, $T_{ri} = L_{ri}/R_{ri}$, $L'_{si} = L_{si} - L_{mi}^2/L_{ri}$. R_{ri}, and R_{si} are DFIG rotor and stator resistances respectively. L_{si}, L_{ri} and L_{mi} are stator, rotor and mutual inductances, respectively.

Drive Train Model of the Turbine-DFIG [7], [41]

$$2H_{ti}\dot{\omega}_{ti} = (T_{ti} - T_{shi}) \quad \text{(A8)}$$

$$2H_{gi}\dot{\omega}_{ri} = (T_{shi} - T_{ei}) \quad \text{(A9)}$$

$$\dot{\theta}_{twi} = \omega_B(\omega_{ti} - \omega_{ri}) \quad \text{(A10)}$$

T_{ti}, T_{shi} and T_{ei} are the turbine, shaft and electrical torque, respectively, given as follows.

$$T_{shi} = k_{shi}\theta_{twi} + c_{shi}\dot{\theta}_{twi} \quad \text{(A11)}$$

$$T_{ei} = \left(E'_{qi}I_{qsi} + E'_{di}I_{dsi}\right)/\omega_s\,,\; T_{ti} = k_i v_w^3 \quad \text{(A12)}$$

where, $T_{ti} = P_{ti}/\omega_{ti}$ is the input turbine torque and P_{ti} is the turbine power in per unit. Two different models have been used to incorporate backlash in the literature by modifying the equation of the shaft torque T_{shi} as follows.

RSC Active Power Loop [41]

$$\dot{x}_{\mathrm{P}i} = \mathrm{P}_{ei}^* - \mathrm{P}_{ei} \quad \text{(A13)}$$

$$\dot{x}_{\mathrm{I}_{qr}i} = k_{\mathrm{P}i}(\mathrm{P}_{ei}^* - \mathrm{P}_{ei}) + \tau_{\mathrm{P}i}^{-1}k_{\mathrm{P}i}x_{\mathrm{P}i} - I'_{qri} \quad \text{(A14)}$$

$$\mathrm{V}'_{qri} = k_{I_{qi}}(k_{\mathrm{P}i}(\mathrm{P}_{ei}^* - \mathrm{P}_{ei}) + \tau_{\mathrm{P}i}^{-1}k_{\mathrm{P}i}x_{\mathrm{P}i} - I'_{qri} + \tau_{\mathrm{I}_{qr}i}^{-1}x_{\mathrm{I}_{qr}i})$$

Authorized licensed use limited to: UNIVERSITY OF SOUTHAMPTON. Downloaded on February 13,2024 at 09:11:53 UTC from IEEE Xplore. Restrictions apply.
© 2023 IEEE. Personal use is permitted, but republication/redistribution requires IEEE permission. See https://www.ieee.org/publications/rights/index.html for more information.

This article has been accepted for publication in IEEE Transactions on Power Systems. This is the author's version which has not been fully edited and content may change prior to final publication. Citation information: DOI 10.1109/TPWRS.2023.3330604

(A15)

RSC Reactive Power Loop [41]

$$\dot{x}_{\mathrm{Q}i} = \mathrm{Q}^{*}_{Si} - \mathrm{Q}_{Si} \quad \text{(A16)}$$

$$\dot{x}_{\mathrm{I}_{dr}i} = k_{\mathrm{Q}i}(\mathrm{Q}^{*}_{Si} - \mathrm{Q}_{Si}) + \tau_{\mathrm{Q}i}^{-1} k_{\mathrm{Q}i} x_{\mathrm{Q}i} - I'_{dri} \quad \text{(A17)}$$

$$\mathrm{V}'_{dri} = k_{I_{d}i}(k_{\mathrm{Q}i}(\mathrm{Q}^{*}_{Si} - \mathrm{Q}_{Si}) + \tau_{\mathrm{Q}i}^{-1} k_{\mathrm{Q}i} x_{\mathrm{Q}i} - I'_{dri} + \tau_{I_{dr}i}^{-1} x_{\mathrm{I}_{dr}i}) \quad \text{(A18)}$$

GSC Active Power Loop [41]

$$\dot{x}_{\mathrm{V_{DC}}i} = \mathrm{V}^{*}_{\mathrm{DC}i} - \mathrm{V}_{\mathrm{DC}i} \quad \text{(A19)}$$

$$\mathrm{V}'_{dgi} = -\mathrm{X}_{Ci}(k_{\mathrm{DC}i}(V^{*}_{\mathrm{DC}i} - V_{\mathrm{DC}i}) + k'_{\mathrm{DC}i} x_{\mathrm{V_{DC}}i}) \quad \text{(A20)}$$

GSC Reactive Power Loop [41], [42]

$$\dot{x}_{\mathrm{Q_{GSC}}i} = \mathrm{Q}^{*}_{\mathrm{GSC}i} - \mathrm{Q}_{\mathrm{GSC}i} \quad \text{(A21)}$$

$$\mathrm{V}'_{qgi} = \mathrm{X}_{Ci}\left(k_{\mathrm{GSC}i}(\mathrm{Q}^{*}_{\mathrm{GSC}i} - \mathrm{Q}_{\mathrm{GSC}i}) + k'_{\mathrm{GSC}i} x_{\mathrm{Q_{GSC}}i}\right) - (\mathrm{V}^{*}_{ti} - \mathrm{V}_{ti}) \quad \text{(A22)}$$

$$\mathrm{V}^{2}_{ti} = \mathrm{V}^{2}_{dsi} + \mathrm{V}^{2}_{dsi} \quad \text{(A23)}$$

$$I_{dgi} = X_{Ci}^{-1}(V_{dgi} - V_{dsi}) \quad \text{(A24)}$$

$$I_{qgi} = -X_{Ci}^{-1}(V_{qgi} - V_{qsi}) \quad \text{(A25)}$$

$$I'_{qgi} + jI'_{dgi} = \left(I_{qgi} + jI_{dgi}\right) e^{-j\theta_{pli}} \quad \text{(A26)}$$

$$I'_{qri} + jI'_{dri} = \left(I_{qri} + jI_{dri}\right) e^{-j\theta_{pli}} \quad \text{(A27)}$$

$$\mathrm{V}_{qgi} + j\mathrm{V}_{dgi} = \left(\mathrm{V}'_{qgi} + j\mathrm{V}'_{dgi}\right) e^{j\theta_{pli}} \quad \text{(A28)}$$

$$\mathrm{V}_{qri} + j\mathrm{V}_{dri} = \left(\mathrm{V}'_{qri} + j\mathrm{V}'_{dri}\right) e^{j\theta_{pli}} \quad \text{(A29)}$$

APPENDIX-B

Synchronous Machine Data, [40]
System Base=100MVA
Individual WTG Power Rating = 5MW
WTG Structural Parameters [19]-[21]

Type-3 WTG Parameters, [6]-[7], [15]
Parameters (in $p.u.$) for $i = 3$ are given below:
$L_{mi} = 4,\ R_{si} = 0.005,\ L_{ri} = 4.06,\ H_{ti} = 4,\ H_{gi} = 0.4,\ R_{ri} = 0.0055,\ \omega_{si} = 1,\ k_{shi} = 0.3,\ c_{shi} = 0.01,\ L_{si} = 4.04,\ k_{pli1} = 100,\ k_{pli2} = 680,\ k_{pli3} = 40,\ k_{wri} = -150,\ \tau_{Bi} = 0.1,\ k_{Pi} = -1.5,\ \tau_{Pi} = 0.025,\ k_{I_q i} = -2.5,\ \tau_{\mathrm{I}_{qr}i} = 0.025,\ k_{\mathrm{Q}i} = 1,\ \tau_{\mathrm{Q}i} = 0.05,\ k_{I_d i} = -2.5,\ \tau_{\mathrm{I}_{dr}i} = 0.05,\ k_{\mathrm{DC}i} = 0.25,\ k'_{\mathrm{DC}i} = 0.1,\ k_{\mathrm{GSC}i} = 0.25,\ k'_{\mathrm{GSC}i} = 0.1,\ \mathrm{X}_{Ci} = 0.55,\ \varrho_i = 0.075$

REFERENCES

[1] IRENA, Renewable Energy Now Accounts for a Third of Global Power Capacity. Accessed on: Apr. 17 2021: https://www.irena.org/newsroom/pressreleases/2019/Apr/Renewable-Energy-Now-Accounts-for-aThird-of-Global-Power-Capacity.

[2] Wind energy in Europe: Scenarios for 2030. http://www.ewea.org/

[3] N. Hatziargyriou et al., "Definition and classification of power system stability revisited & extended," *IEEE Trans. Power Syst*., 2020.

[4] D. Gautam, V. Vittal, and T. Harbour, "Impact of increased penetration of DFIG-based wind turbine generators on transient and small signal stability of power systems," *IEEE Trans. Power Syst*., vol. 24, no. 3, pp. 1426–1434, Aug. 2009.

[5] I. A. Hiskens, "Dynamics of Type-3 Wind Turbine Generator Models," *IEEE Trans. Power Syst*., vol. 27, no. 1, pp. 465-474, Feb. 2012.

[6] G. P. Prajapat, N. Senroy, and I. N. Kar, "Wind Turbine Structural Modeling Consideration for Dynamic Studies of DFIG Based System," *IEEE Trans. Sustain. Energy*, vol. 8, no. 4, pp. 1463–1472, 2017.

[7] F. Mei and B. C. Pal, "Modal analysis of grid connected doubly fed induction generator," *IEEE Trans. Energy Convers*., vol. 22, no. 3, pp. 728–736, Sep. 2007.

[8] L. Yang, Z. Xu, J. Østergaard, Z. Y. Dong, K. P. Wong and X. Ma, "Oscillatory Stability and Eigenvalue Sensitivity Analysis of A DFIG Wind Turbine System," *IEEE Trans Energy Convers*., vol. 26, no. 1, pp. 328-339, March 2011.

[9] A. S. Mir and N. Senroy, "DFIG damping controller design using robust CKF based adaptive dynamic programming," *IEEE Trans. Sustain. Energy*, vol. 11, no. 2, pp. 839-850, Apr. 2020.

[10] F. M. Hughes, O. Anaya-Lara, N. Jenkins, and G. Strbac, "A power system stabilizer for DFIG-based wind generation," *IEEE Trans. Power Syst*., vol. 21, no. 2, pp. 763–772, May 2006.

[11] A. Tapia, G. Tapia, J. X. Ostolaza, and J. R. Saenz, "Modeling and control of a wind turbine driven doubly fed induction generator," *IEEE Trans. Energy Convers.*, vol. 18, no. 2, pp. 194–204, Jun. 2003.

[12] Y. Lei, A. Mullane, G. Lightbody, and R. Yacamini, "Modeling of the wind turbine with a doubly fed induction generator for grid integration studies," *IEEE Trans. Energy Convers*., vol. 21, no. 1, Mar. 2006.

[13] R. Pena, "A doubly fed induction generator using back to back PWM converters supplying an isolated load from a variable speed wind-energy generation," *IEE Proc. Elect. Power Appl*., vol. 143, no. 3, pp. 231–241, May 1996.

[14] S. K. Salman and A. L. J. Teo, "Windmill modeling consideration and factors influencing the stability of a grid-connected wind power-based embedded generator," *IEEE Trans. Power Syst*., vol. 18, no. 2, pp. 793– 802, May 2003.

[15] Y. Mishra, S. Mishra, F. Li, Z. Y. Dong, and R. C. Bansal, "Small-signal stability analysis of a DFIG-based wind power system under different modes of operation," *IEEE Trans. Energy Convers*., vol. 24, no. 4, pp. 972– 982, Dec. 2009.

[16] K. V. Vidyanandan and N. Senroy, "Primary frequency regulation by deloaded wind turbines using variable droop," *IEEE Trans. Power Syst*., vol. 28, no. 2, pp. 837–846, May 2013.

[17] S. Ghosh and N. Senroy, "Electromechanical dynamics of controlled variable-speed wind turbines," *IEEE Syst. J*., vol. 9, no. 2, Jun. 2015.

[18] R. Fadaeinedjad, M. Moallem, and G. Moschopoulos, "Simulation of a wind turbine with doubly fed induction generator by FAST and simulink," *IEEE Trans. Energy Convers*., vol. 23, no. 2, , Jun. 2008.

[19] A. Staino,"Actuator control of edgewise vibrations in wind turbine blades," *J. Sound Vib*., vol. 331, pp. 1233–1256, Mar. 2012.

[20] O. L. Hansen Martin, *Aerodynamics of Wind Turbines*, 2nd ed. London, U.K.: Earthscan, 2008.

[21] M. A. Lackner and M. Rotea, "Structural control of floating wind turbines," *Mechatronics*, vol. 21, no. 4, pp. 704–719, 2011.

[22] W. Yan, X. Wang, W. Gao and V. Gevorgian, "Electro-mechanical Modeling of Wind Turbine and Energy Storage Systems with Enhanced Inertial Response," *Jour. Modern Power Syst. and Clean Energy*, vol. 8, no. 5, pp. 820-830, September 2020.

[23] S. Ma, H. Geng, G. Yang and B. C. Pal, "Clustering-Based Coordinated Control of Large-Scale Wind Farm for Power System Frequency Support," *IEEE Trans. Sustain. Energy*, vol. 9, no. 4, Oct. 2018.

[24] L. Sun, K. Liu, J. Hu and Y. Hou, "Analysis and Mitigation of Electromechanical Oscillations for DFIG Wind Turbines Involved in Fast Frequency Response," *IEEE Trans. Power Syst*., vol. 34, no. 6, pp. 4547-4556, Nov. 2019.

[25] G. P. Prajapat, P. Bhui, N. Senroy, and I. N. Kar, "Modelling and estimation of gear train backlash present in wind turbine driven DFIG system," *IET Gen., Trans. Dist*., vol. 12, no. 14, pp. 3527–3535, 2018.

[26] G. P. Prajapat, N. Senroy, I.N. Kar, "Modeling and impact of gear train backlash on performance of DFIG wind turbine system," Electric Power Systems Research, Volume 163, Part A, pp. 356 –364, 2018.

[27] L. P. Kunjumuhammed, *et. al*., "The Adequacy of the Present Practice in Dynamic Aggregated Modeling of Wind Farm Systems," *IEEE Trans. Sustain. Energy*, vol. 8, no. 1, pp. 23-32, Jan. 2017.

[28] X. He and H. Geng, "An overview on wind farm modelling for power system stability studies," 8th Renew. Power Gen. Conf, 2019, pp. 1-8.

[29] Y. Li, L. Fan and Z. Miao, "Wind in Weak Grids: Low-Frequency Oscillations, Subsynchronous Oscillations, and Torsional Interactions," *IEEE Trans. Power Syst*., vol. 35, no. 1, pp. 109-118, Jan. 2020.

[30] U. Buragohain and N. Senroy, "Reduced Order DFIG Models for PLL-Based Grid Synchronization Stability Assessment," *IEEE Trans. Power Syst.*, vol. 38, no. 5, pp. 4628-4639, Sept. 2023.

[31] Y. Ma, D. Zhu, Z. Zhang, X. Zou, J. Hu and Y. Kang, "Modeling and Transient Stability Analysis for Type-3 Wind Turbines Using Singular Perturbation and Lyapunov Methods," *IEEE Trans. Ind. Electron*., vol. 70, no. 8, pp. 8075-8086, Aug. 2023.

[32] W. Tang, J. Hu, Y. Chang and F. Liu, "Modeling of DFIG-Based Wind Turbine for Power System Transient Response Analysis in Rotor Speed Control Timescale," *IEEE Trans. Power Syst.*, vol. 33, no. 6, pp. 6795-6805, Nov. 2018.

[33] S. Morovati, Y. Zhang, S. M. Djouadi, K. Tomsovic, A. Wintenberg

Authorized licensed use limited to: UNIVERSITY OF SOUTHAMPTON. Downloaded on February 13,2024 at 09:11:53 UTC from IEEE Xplore. Restrictions apply.
© 2023 IEEE. Personal use is permitted, but republication/redistribution requires IEEE permission. See https://www.ieee.org/publications/rights/index.html for more information.

This article has been accepted for publication in IEEE Transactions on Power Systems. This is the author's version which has not been fully edited and content may change prior to final publication. Citation information: DOI 10.1109/TPWRS.2023.3330604

and M. Olama, "Robust Output Feedback Control Design for Inertia Emulation by Wind Turbine Generators," *IEEE Trans. Power Syst.*, vol. 36, no. 6, pp. 5056-5067, Nov. 2021.
[34] S. Li, H. Zhang, Y. Yan and J. Ren, "Parameter Optimization to Power Oscillation Damper (POD) Considering its Impact on the DFIG," *IEEE Trans. Power Syst.*, vol. 37, no. 2, pp. 1508-1518, March 2022.
[35] S. Vijayshankar, V. Purba, P. J. Seiler and S. V. Dhople, "Reduced-order Aggregate Dynamical Model for Wind Farms," 2019 (ACC), Philadelphia, PA, USA, 2019, pp. 5464-5471.
[36] V. Purba, B. B. Johnson, S. Jafarpour, F. Bullo and S. V. Dhople, "Dynamic Aggregation of Grid-Tied Three-Phase Inverters," *IEEE Trans. Power Syst*., vol. 35, no. 2, pp. 1520-1530, March 2020
[37] C. Nichita, D. Luca, B. Dakyo, and E. Ceanga, "Large band simulation of the wind speed for real time wind turbine simulators," *IEEE Trans. Energy Convers.*, vol. 17, no. 4, pp. 523–529, 2002.
[38] C. Canizares et al., "Benchmark Models for the Analysis and Control of Small-Signal Oscillatory Dynamics in Power Systems," *IEEE Trans. Power Syst*., vol. 32, no. 1, pp. 715–722, 2017.
[39] *IEEE Guide for Synchronous Generator Modeling Practices and Parameter Verification with Applications in Power System Stability Analyses*, IEEE Std 1110-2019, vol., no., pp.1-92, 2 March 2020.
[40] A. K. Singh and B. C. Pal, *Dynamic estimation and control of power systems*, First edit. Elsevier Inc., 2018.
[41] G. Abad, J. Lopez, M. A. Rodriguez, L. Marroyo and G. Iwanski, *Doubly Fed Induction Machine Modeling and Control for Wind Energy Generation Applications*, Hoboken, NJ, USA:Wiley, 2011.
[42] A. Nagliero, R. A. Mastromauro, M. Liserre, and A. Dell'Aquila, "Synchronization techniques for grid connected wind turbines," in *Proc. 35th Annu. Conf. IEEE Ind. Electron.*, Nov. 2009, pp. 4606–4613.
[43] N. Chaudhuri, B. Chaudhuri, R. Majumder, and A. Yazdani, *Multi-Terminal Direct-Current Grids: Modeling, Analysis, and Control*. Hoboken, NJ, USA: John Wiley & Sons, 2014.
[44] M. Nordin and P. Gutman, "Controlling mechanical systems with backlash— a survey," *Automatica*, vol. 38, pp. 1633–1649, 2002.
[45] M. Nordin, and J. Galic, New models for backlash and gear play. Int J. of Adaptive Control and Signal Processing, 1:9-63, 1997.
[46] I. N. Kar, T. Miyakura, and K. Seto, "Bending and torsional vibration control of a flexible plate structure using H∞-based robust control law," *IEEE Trans. Control Syst. Technol.*, vol. 8, no. 3, pp. 545–553, 2000.
[47] J. Margielewicz, D. Gaska, and G. Litak, "Modelling of the gear backlash," Nonlinear Dyn., vol. 97, no. 1, pp. 355–368, 2019
[48] J. Hu, "Modeling of grid-connected DFIG-based wind turbines for DC-link voltage stability analysis," *IEEE Trans. on Sustain. Energy*, vol. 6, no. 4, pp. 1325-1336, Oct. 2015.
[49] Y. Liu et al., "Dynamic State Estimation for Power System Control and Protection," *IEEE Trans. Power Syst.*, vol. 36, no. 6, pp. 5909-5921, Nov. 2021
[50] G. Tu, Y. Li and J. Xiang, "Coordinated Rotor Speed and Pitch Angle Control of Wind Turbines for Accurate and Efficient Frequency Response," *IEEE Trans. Power Syst*., vol. 37, no. 5, Sept. 2022.

Abdul Saleem Mir (S'19–M'22) received his Ph.D. degree in Electrical Engineering from Indian Institute of Technology Delhi, India, in 2020. He is currently an Assistant Professor in the Department of Electrical Engineering, Indian Institute of Technology Roorkee, India. He is a member of IEEE PES Task Force on Standard Test Cases for Power System State Estimation. He was awarded IEEE PES Working Group Awards in 2022/2023 for his contributions to IEEE PES TF on Dynamic State and Parameter Estimation. His research interests include DSE based control, power system dynamics and modeling/control of DERs.

Abhinav Kumar Singh (S'12–M'15) received his B. Tech. degree in Electrical Engg. from Indian Institute of Technology Delhi, India, and Ph.D. degree in EE from Imperial College London, U.K. in 2010 and 2015 respectively. He is a Lecturer at the School of Electronics and Computer Science, University of Southampton. Previously, he was a Lecturer at the University of Lincoln from Aug 2017 to Mar 2019, and a Research Associate at Imperial College London from Jan 2015 to July 2017. He won IEEE PES Working Group Recognition Award in 2016 for his contributions to IEEE PES task force on benchmark systems. He was awarded IEEE PES Working Group Recognition Awards in 2016 and 2022 for his contributions to two IEEE PES Task Forces. He is a member of IEEE PES Task Force on Dynamic State and Parameter Estimation and IEEE PES Task Force on Standard Test Cases for Power System State Estimation. His research interests include real-time estimation and control of future energy networks.

Nilanjan Senroy (S'01–M'06-SM'18) received the B. Tech. degree from the National Institute of Technology, Jamshedpur, India, and the M.S. and Ph.D. degrees from Arizona State University, Tempe, AZ, USA. He also has postdoctoral experience at the Center for Advanced Power Systems, Florida State University, Tallahassee, FL, USA. He is currently Power Grid Chair Professor in the Department of Electrical Engineering, Indian Institute of Technology Delhi, India. He currently serves as an Editor of IEEE Transactions on Power Systems and IEEE PES Letters. His research interests include power system stability and control, dynamics, modeling and simulation of wind energy conversion systems and signal processing techniques in power systems.

Bikash C. Pal (M'00-SM'02-F'13) received B.E.E. degree (with honors) from Jadavpur University, Calcutta, India, M.E. degree from the Indian Institute of Science, Bangalore, India, and Ph.D. degree from Imperial College London, London, U.K., in 1990, 1992, and 1999, respectively, all in electrical engineering. Currently, he is a Professor in the Department of Electrical and Electronic Engineering, Imperial College London. His research interests include renewable energy modelling and control, state estimation, and power system dynamics. He is Vice President Publications, IEEE Power & Energy Society. He was Editor-in-Chief of IEEE Transactions on Sustainable Energy (2012-2017) and Editor-in-Chief of IET Generation, Transmission and Distribution (2005-2012) and is a Fellow of IEEE for his contribution to power system.

Authorized licensed use limited to: UNIVERSITY OF SOUTHAMPTON. Downloaded on February 13,2024 at 09:11:53 UTC from IEEE Xplore. Restrictions apply.
© 2023 IEEE. Personal use is permitted, but republication/redistribution requires IEEE permission. See https://www.ieee.org/publications/rights/index.html for more information.